

Spin Dependence in Proton-Proton Elastic Scattering at RHIC

S. Bültmann, I. H. Chiang, R. E. Chrien, A. Drees, R. L. Gill, W. Gury^{*},
J. Landgraf, T. A. Ljubičić, D. Lynn, C. Pearson, P. Pile, A. Rusek,
M. Sakitt, B. Surrow, S. Tepikian
Brookhaven National Laboratory, USA

J. Chwastowski, B. Pawlik
Institute of Nuclear Physics, Poland

M. Haguenaue
Ecole Polytechnique, Palaiseau, France

A. A. Bogdanov, S. B. Nurushev, M. F. Runtzo, M. N. Strikhanov
Moscow Engineering Physics Institute, Russia

I. G. Alekseev, V. P. Kanavets, L. I. Koroleva, B. V. Morozov, D. N. Svirida
Institute for Theoretical and Experimental Physics, Russia

A. Khodinov, M. Rijssenbeek, L. Whitehead
Stony Brook University, USA

K. De, N. Öztürk
University of Texas at Arlington, USA

A. Sandacz
Institute for Nuclear Studies, Poland

^{*}Spokesperson: BNL Physics Department, Upton, NY 11973-5000, USA
Phone: 1-631-344-3878, E-mail: gury@bnl.gov

Statement of basic requirements

Proton beams with transverse polarization at RHIC are required for this experiment, which is already installed at the 2 O'clock IP at RHIC. The existing and commissioned Roman Pot systems shall be used. Our computing and network is already in place, and the needs in this area are minimal. Three phases of the experiment and their needs are described in the Executive Summary on the following page.

August 2003

Executive Summary

We are proposing a comprehensive experiment to measure spin dependence of proton-proton elastic scattering at RHIC in the totally unexplored region of center of mass energy \sqrt{s} and four momentum transferred $|t|$. Our proposal is to run at the two energies, which are part of the running of RHIC Spin: $\sqrt{s} = 200$ GeV and $\sqrt{s} = 500$ GeV. Taking advantage of already existing and debugged equipment of the pp2pp experiment we are proposing to accomplish the goals of the experiment in three phases, starting with the Phase 1, for which only miscellaneous costs of \$ 25k are needed.

Phase 1: Running with the current setup we will measure and study the spin dependence of elastic scattering at $\sqrt{s} = 200$ GeV with $\beta^* = 20$ m and $\sqrt{s} = 500$ GeV with $\beta^* = 10$ m. The A_N , A_{NN} , $d\sigma/dt$, and σ_{tot} will be measured at both energies and ρ at $\sqrt{s} = 200$ GeV. The suitable $|t|$ interval at $\sqrt{s} = 200$ GeV is $0.003 < |t| < 0.02$ (GeV/c)². The error of $\Delta A_N = 0.004$ for each of the six data points in the above $|t|$ interval can be obtained. The expected error on the slope parameter $\Delta b = 0.3$ (GeV/c)⁻² and on the ratio of real to imaginary part of the scattering amplitude $\Delta\rho = 0.01$.

At $\sqrt{s} = 500$ GeV A_N can be measured with the same errors. However, since the useful absolute $|t|$ interval is $0.025 < |t| < 0.12$ (GeV/c)², which is far from the CNI region, one can measure b with $\Delta b \approx 0.3$. The cost of miscellaneous items for this phase is about \$ 25k. Our request is for three days of data taking at each of the two energies of $\sqrt{s} = 200$ GeV and $\sqrt{s} = 500$ GeV.

Phase 2: Running with Roman Pots in the DX-D0 region, we will extend the $|t|$ range at $\sqrt{s} = 200$ GeV to 0.2 (GeV/c)² and to study the diffractive minimum region and its spin dependence at $\sqrt{s} = 500$ GeV to 1.3 (GeV/c)². The additional cost for the modification of DX-D0 region and new Roman Pot stations, while using the existing detectors, is estimated to be \$ 452k. No dedicated running time is required for this phase, because no special conditions are required.

Phase 3: Extend the $|t|$ range into the Coulomb region of elastic scattering to make precision measurements, as outlined in the original proposal, of ρ , σ_{tot} , and the spin dependence of $\Delta\sigma_{tot}$. With that setup detailed information of helicity amplitudes at small $|t|$ will shed light on σ_{tot} . Given the data sample of six million elastic events the statistical accuracy of the measurement of σ_{tot} is better than 1%. Therefore, the ultimate error will be limited by the systematic uncertainty on the luminosity and beam transport. Cost of the power supplies for this phase is \$ 362k. We expect two days of time for data taking at each energy plus setup time of the beam optics.

Contents

1	Introduction	1
1.1	Physics Overview	1
1.2	Spin Dependence of Elastic Scattering	2
1.3	Unpolarized Elastic Scattering at Small $ t $	9
1.4	Scattering at Medium Momentum Transfer	11
2	Accomplishments to Date of pp2pp	16
2.1	Existing pp2pp Equipment	16
2.2	Overview of the Experimental Technique	17
2.2.1	Transport Theory	17
2.2.2	Actual Beam Transport	19
2.2.3	Measurement of the Beam Angle and Position at the IP	20
2.2.4	Silicon Strip Detector	21
2.3	The Engineering Run in 2002	22
2.4	The Data Taking Run in 2003	23
3	Proposed Plan for the Experiment	26
3.1	Phase 1: Running with the current setup	26
3.2	Phase 2: Medium $ t $ Region	29
3.3	Phase 3: CNI Region	32
4	Cost and Proposed Run Plan	34
A	pp2pp Paper	36
B	Bibliography	42

Chapter 1

Introduction

In this new proposal, we are asking for continuation of data taking with the existing and debugged equipment of the pp2pp experiment, which already has had two very productive data taking periods: An engineering run in 2002 and a data taking run in 2003. In Chapter 2 we will describe the accomplishments of the two running periods that we had at RHIC. We outline the physics measurements that can be made with our setup and the physics motivation for making them. We also outline what additional resources are needed to accomplish most of the goals of the pp2pp experiment as described in the original proposal [1] and presented to the Physics Advisory Committee (PAC) in 1994 and also in 1995. Our projections are based on our actual experience of running at RHIC.

The pp2pp experiment was approved by the management of the Brookhaven National Laboratory after the recommendation of the PAC in 1994. The approval was re-confirmed in 1995 following an update review of the experiment in that year. In his letter to the pp2pp Collaboration of June 10, 2003 the experiment was declared completed by Dr. T. Kirk “...purpose of this letter is to formally declare that Experiment R7 is complete at this point in time and will not be scheduled for further data taking at RHIC.”

Our request for continuation has a significant merit. RHIC provides a unique opportunity to study spin dependence of elastic and diffractive collisions of polarized protons at center-of-mass energies up to 500 GeV. A sizable investment, that has been already made, will allow us to achieve many physics goals with only relatively short running periods. Those can be allocated, for example, at the end of the commissioning runs of RHIC Spin. In Chapter 3 we outline how staging of the experiment with and/or without additional capital investment will result in achieving the remaining physics goals outlined in the original proposal: The measurement of the differential cross section for different spin states in a wide range of \sqrt{s} and $|t|$. In Chapter 4 we will summarize cost and schedule.

1.1 Physics Overview

RHIC with its capability of colliding polarized proton beams is a unique place to study elastic scattering and its spin dependence, allowing to investigate the accepted theory of strong interactions, Quantum Chromo Dynamics (QCD), in the nonperturbative regime. QCD has

been very successful in describing hadronic interactions at large four-momentum-transfer squared $|t|$. For small $|t|$ values of elastic scattering however, the theory has not been as successful. This is the regime of soft hadronic interactions where phenomenological models, constrained by asymptotic theorems, are used to explain the nature of the hadronic interaction.

The highest \sqrt{s} energy at which these experimental studies were performed in proton-proton collisions was 62.8 GeV at the CERN ISR using unpolarized beams, and 20 GeV with polarized beams. The pp2pp experiment extends these measurements over a wide range of energy and four-momentum transfer up to $\sqrt{s} = 500$ GeV. In this "data-driven" field, having more experimental results is important. The existing data on pp and $p\bar{p}$ are not sufficient to understand the exchange process at high energies in detail. For example, the direct measurement which avoids all uncontrollable uncertainties can test the postulate that at high energies the difference between pp and $p\bar{p}$ cross section is negligible. Moreover, polarization studies in the RHIC energy range will be of utmost interest in order to explore the emerging new picture of diffraction and its spin dependence. The strength of what we propose is that many aspects of spin dependence in proton-proton elastic scattering is related to what is measured with unpolarized beams.

The insights gained in this experiment will have consequences for many other experiments, for example HERA, Tevatron and LHC where in wide rapidity gap events one or both vertices of the interaction, namely proton-Pomeron vertex, are the same as in proton-proton elastic scattering.

In general, the physics of our experiment is naturally divided into two $|t|$ regions:

1. In the small $|t|$, CNI region, $0.0005 < |t| < 0.12$ (GeV/c)², we will measure and study the differential cross section as a function of \sqrt{s} and initial transverse spin state, which yields the analyzing power A_N , the double spin correlation parameter A_{NN} , the difference of the spin dependent total cross sections $\Delta\sigma_T$, the total and elastic cross sections σ_{tot} and σ_{el} , the ratio of the real to the imaginary part of the forward elastic scattering amplitude ρ , and the nuclear slope parameter of pp elastic scattering b .
2. In the intermediate $|t|$ region, $|t| \leq 1.3$ (GeV/c)², we plan to study the evolution of the dip structure with \sqrt{s} , as observed at ISR in the differential elastic cross section, $d\sigma_{el}/dt$, and the s and $|t|$ dependence of b . One of the interesting features observed experimentally is a correlation between the position of the dip and the single spin asymmetry A_N crossing zero at the same $|t|$ value.

By measuring spin asymmetries in the $|t|$ range of this experiment, we will be able to constrain the helicity amplitudes ϕ_i , which describe elastic scattering. Those amplitudes are not very well known at this time. In the following sections we elaborate on these topics.

1.2 Spin Dependence of Elastic Scattering

RHIC has the unique capability of accelerating polarized protons, which will enable us to measure the spin dependent parameters of elastic pp scattering at much higher cms energies

compared to the highest energy data to date at $\sqrt{s} = 24$ GeV. Those measurements were performed using a polarized target with unpolarized incident protons. There has been a recent revival of interest in the elastic pp scattering with polarized protons which covers a large spectrum of interesting physics. For instance, the intimate relationship between a sharp zero-crossing of the analyzing power and the dip region in the elastic differential cross section has continued to be the focus of a number of studies.

The main polarization measurements to be performed with polarized protons in elastic interactions are listed below. We assume here that only transverse proton polarization is available at the IP of the proposed experiment:

1. the analyzing power A_N ;
2. the difference in the total cross section as a function of initial transverse spin states $\Delta\sigma_T = \sigma_{tot}^{\uparrow\downarrow} - \sigma_{tot}^{\uparrow\uparrow}$;
3. the transverse double spin correlation parameter A_{NN} .

The kinematical region covers $4 \times 10^{-4} \leq |t| \leq 1.3 (\text{GeV}/c)^2$. There is a pronounced lack of data in the region from $0.05 (\text{GeV}/c)^2$ to $0.15 (\text{GeV}/c)^2$ as can be seen in Figure 1.1.

In the 1970's the failure of simple Regge models to explain polarization data resulted in the introduction of absorption corrections, but at the same time this inevitable approach reduced the interest in these models. At present, however, the framework is quite different, since much theoretical work has been done in connecting the Regge phenomenology to QCD concepts [2] by associating Pomeron (P) exchange with the exchange of $n \geq 2$ (non-perturbative) gluons [3, 4, 5]. For the case $n = 2$ ($C = +1$), this mechanism generates a bare hard Pomeron, while for $n = 3$, containing both $C = \pm 1$, the $C = -1$ amplitude leads to the bare Odderon (O), corresponding to an odd-signature partner of P [6, 7, 8, 9, 10, 11, 12].

In discussing the polarization data, the s -channel helicity amplitudes [13] for pp elastic scattering ϕ_i ($i = 1 - 5$) are used. It is somewhat more convenient to express these in combinations that explicitly exhibit the t -channel exchange characteristics at high energy:

$$\begin{aligned}
\phi_1(s, t) &= \langle ++ | M | ++ \rangle, \\
\phi_2(s, t) &= \langle ++ | M | -- \rangle, \\
\phi_3(s, t) &= \langle +- | M | +- \rangle, \\
\phi_4(s, t) &= \langle +- | M | -+ \rangle, \\
\phi_5(s, t) &= \langle ++ | M | +- \rangle.
\end{aligned} \tag{1.1}$$

The analyzing power A_N can be expressed in terms of these amplitudes as:

$$A_N \frac{d\sigma}{dt} = -\frac{4\pi}{s^2} \text{Im}[\phi_5^*(\phi_1 + \phi_2 + \phi_3 - \phi_4)] \tag{1.2}$$

where the spin-averaged differential cross section is:

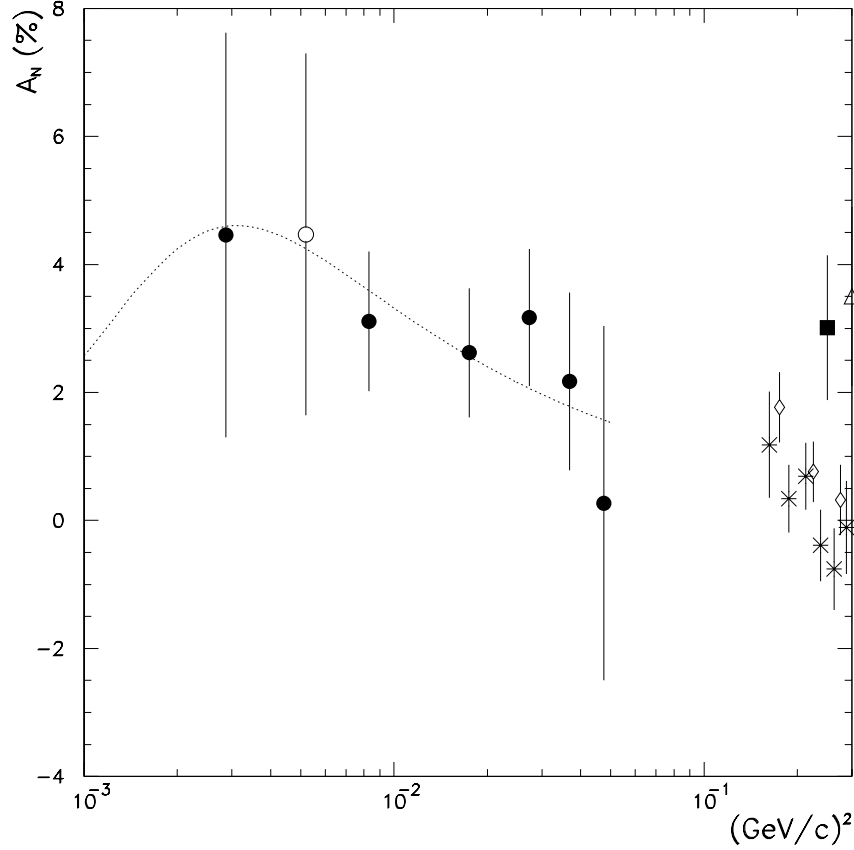


Figure 1.1: A_N data for pp elastic scattering as a function of $|t|$. The dotted curve is the theoretical prediction [14] in the Coulomb-nuclear region. \circ is measured at 185 GeV/c [34] and the filled circles are measured with 200 GeV/c [35]. The other data points are measured at 300 GeV/c (cross) and 100 GeV/c (diamond) [20], 176 ± 12 GeV/c (triangle) [21] and at 150 GeV/c (black square) [19], using a polarized target.

$$\frac{d\sigma}{dt} = \frac{2\pi}{s^2} [|\phi_1|^2 + 2|\phi_2|^2 + |\phi_3|^2 + |\phi_4|^2 + 4|\phi_5|^2] \quad (1.3)$$

and the total cross section is:

$$\sigma_{tot} = \frac{4\pi}{s} \text{Im}[\phi_1(s, t) + \phi_3(s, t)]|_{t=0} \quad (1.4)$$

The double-spin asymmetry parameter is expressed as:

$$A_{NN} \frac{d\sigma}{dt} = \frac{4\pi}{s^2} [2|\phi_5|^2 + \text{Re}(\phi_1^* \phi_2 - \phi_3^* \phi_4)] \quad (1.5)$$

There are several specific $|t|$ regions to be investigated in polarized pp scattering:

1. Forward direction, $|t| \simeq 0$ region, is relevant to the total cross-section measurements σ_{tot} and $\Delta\sigma_T$.
2. Analyzing power in the CNI region: The electromagnetic and hadronic amplitudes are of comparable magnitude in the very forward direction, and this results in a small but significant asymmetry A_N in pp scattering near the point of maximum interference. The asymmetry has a characteristic shape, first calculated by Schwinger and subsequently by other authors [14, 15, 16, 17, 18]. The interference between the hadronic non-flip and the electromagnetic spin-flip amplitudes gives rise to this asymmetry. The electromagnetic single-flip amplitude, ϕ_5^{em} , is real and is calculated in one-photon exchange approximation:

$$\phi_5^{em} = \frac{\alpha\sqrt{s}\mu_p - 1}{\sqrt{|t|} 2m} \quad (1.6)$$

where α is the fine structure constant and μ_p is the proton's total magnetic moment. Consequently, the analyzing power is a function of the total cross section and the momentum-transfer, with a maximum of A_{max} at $t = t_{max}$ and can be written as

$$\begin{aligned} A_N &= \frac{\frac{\alpha}{2m}(\mu_p - 1)\frac{\sigma_{tot}}{\sqrt{|t|}}}{\frac{\sigma_{tot}^2}{16\pi} + \frac{4\pi\alpha^2}{t^2}} \\ &= A_{max} \frac{4z^{3/2}}{3z^2 + 1} \end{aligned} \quad (1.7)$$

where $z = t/t_{max}$ and $t_{max} = \sqrt{3} \frac{8\pi\alpha}{\sigma_{tot}} = 2 \times 10^{-3} \text{ (GeV}/c)^2$ for pp total cross section $\sigma_{tot} = 60 \text{ mb}$ and $A_{max} = \frac{\sqrt{3}}{4} (\mu_p - 1) (\sqrt{t_{max}}/m) = 0.037$. These numbers are appropriate for RHIC energies at $\sqrt{s} = 500 \text{ GeV}$, and are somewhat different from those obtainable from the lower energy data shown in Figure 1.1. The results are consistent with the theoretical prediction, but an experiment with better event statistics is needed to accurately fit the $|t|$ dependence down to $5 \times 10^{-4} \text{ (GeV}/c)^2$.

3. It would be beneficial to cover systematically the $|t|$ region of 0.05 to 0.15 $(\text{GeV}/c)^2$ in order to disentangle the possible spin dependent amplitudes that survive at high energies even in the small $|t|$ region. This would provide the much needed input to the theoretical studies of pp elastic scattering amplitudes.
4. The $|t|$ region where the dip was found to develop, starting around $\sqrt{s} \approx 15 \text{ GeV}$, shows a unique structure in A_N . This region needs to be further explored by also measuring the double-spin correlation parameter A_{NN} .
5. The region for $|t| > 2 \text{ (GeV}/c)^2$ is essentially unexplored and high precision measurements can shed light on the possible onset of a *hard* regime spin effects.

As noted earlier, polarization measurements in elastic scattering have only been performed with a fixed target up to 300 GeV/c ($\sqrt{s} = 24$ GeV). When the polarization asymmetry results for pp elastic scattering at 100 - 300 GeV/c beam momenta [19, 20, 21, 22, 23] and other lower energy experiments [24, 25, 26, 27, 28, 29] are considered together over the full measured $|t|$ range, they exhibit the following general features (see Figure 1.2):

1. The analyzing power A_N at small $|t|$ values ($|t| \leq 0.5$ (GeV/c)²) is positive and decreasing like $\sim 1/\sqrt{s}$ up to $s \approx 50$ GeV², with a possible flattening around values of a few percent up to the highest energies.
2. For $s \geq 50$ GeV², A_N changes sign in the $|t|$ range between 0.4 and 1.0 (GeV/c)² reaching a negative minimum followed by a sharp zero-crossing in the region where the diffractive dip in the differential cross section develops around $|t| \approx 1.2$ (GeV/c)², possibly remaining positive at larger $|t|$ values.

The features outlined above have stimulated a number of discussions on a possible hadronic spin-flip contribution $\phi_5^{(h)}$ that does not necessarily decrease as $1/\sqrt{s}$. It was suggested that diffractive scattering with exchange of two pions could become important at large s ; this mechanism can cause a non-vanishing $\phi_5^{(h)}$ because one of the two pions can couple with spin-flip, while the other does not [30]. It was also pointed out that $\phi_5^{(h)}$ might remain non-zero at high energies if the nucleon contains a dynamically enhanced compact diquark component [16].

In order to clarify the issue of diffractive (Pomeron) spin-flip, it would be important to have more precise polarization asymmetry data in the low $|t|$ region [31]. There is no measurement to this day in the range of $0.05 \leq |t| \leq 0.15$ (GeV/c)². This deficiency has also been pointed out in [32] where small-angle polarization is discussed in terms of non-perturbative instanton-like contributions of the gluonic field. In more general terms, it has also been suggested that, with the injection of QCD concepts in the picture of elastic scattering, the kinematic region $|t| \approx \Lambda_{QCD}^2$ ($\Lambda_{QCD} = 0.15$ GeV/c) might be of special interest [33].

With both RHIC colliding beams polarized, the double-spin correlation parameter A_{NN} can be measured up to rather large $|t|$ values. In this case, it will also be possible to investigate the puzzling observations of large differences between parallel and antiparallel spin cross-sections observed at ZGS around 12 GeV/c. From these measurements it appears that two protons interact harder when their spins are parallel. However, it is not clear if this effect persists at high energies.

First we list the differential counting rates N as functions of initial spin orientations:

$$N_{\uparrow\uparrow}(t) = \mathcal{L} \frac{d\sigma}{dt} \{1 + A_N(P_1 + P_2) \cos \phi + A_{NN} P_1 P_2 \cos^2 \phi\}, \quad (1.8)$$

$$N_{\downarrow\downarrow}(t) = \mathcal{L} \frac{d\sigma}{dt} \{1 - A_N(P_1 + P_2) \cos \phi + A_{NN} P_1 P_2 \cos^2 \phi\}, \quad (1.9)$$

$$N_{\uparrow\downarrow}(t) = \mathcal{L} \frac{d\sigma}{dt} \{1 + A_N(P_1 - P_2) \cos \phi - A_{NN} P_1 P_2 \cos^2 \phi\}, \quad (1.10)$$

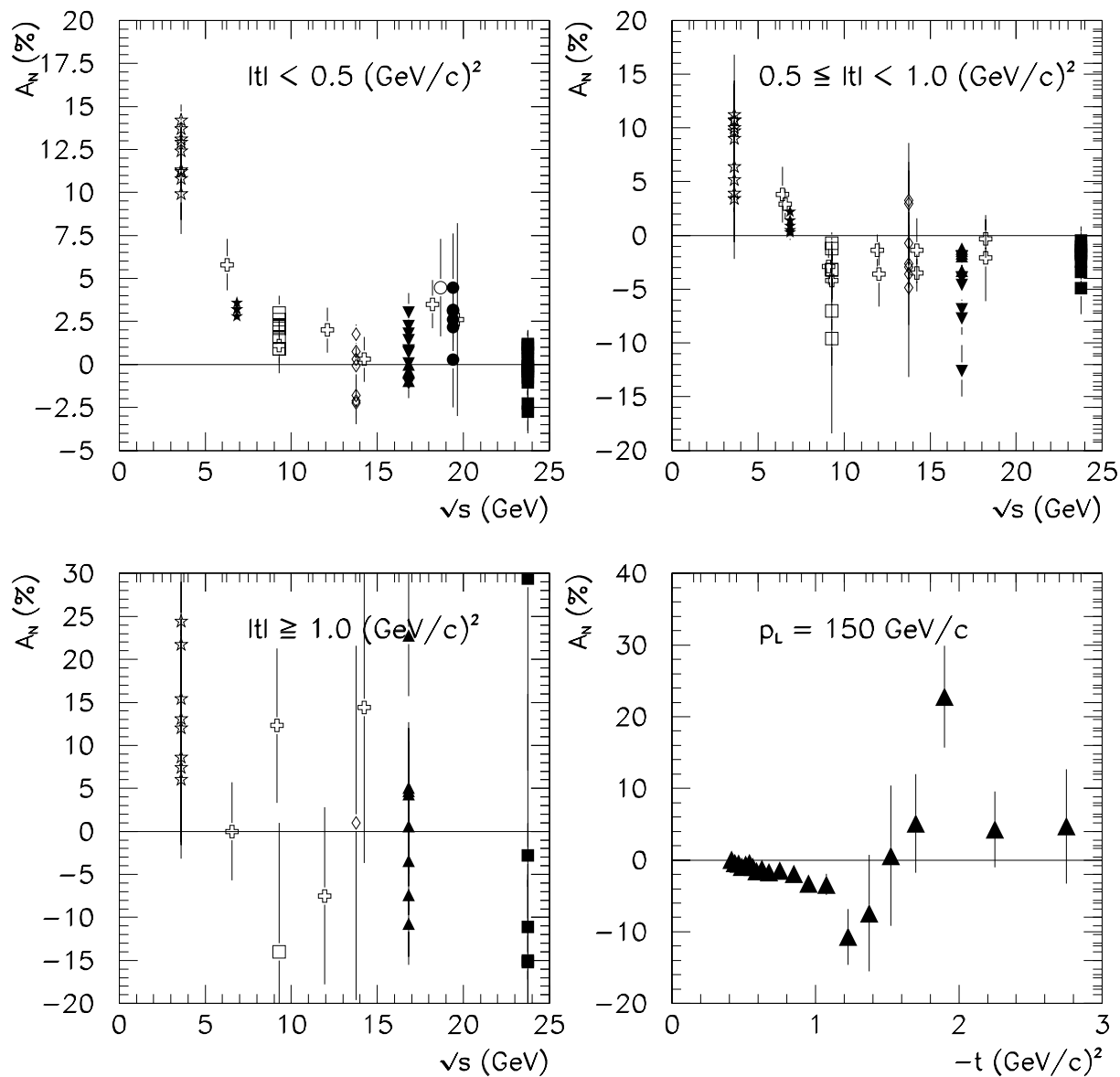


Figure 1.2: A_N data for pp elastic scattering as a function of center-of-mass energy in three different $|t|$ regions. The data points span 6 - 300 GeV/c incident lab momenta. Note that, as the $|t|$ increases above 1 (GeV/c)², the data points have larger error bars and they are more scattered. In the lower $|t|$ ranges, however, A_N is positive and decreases like $1/\sqrt{s}$.

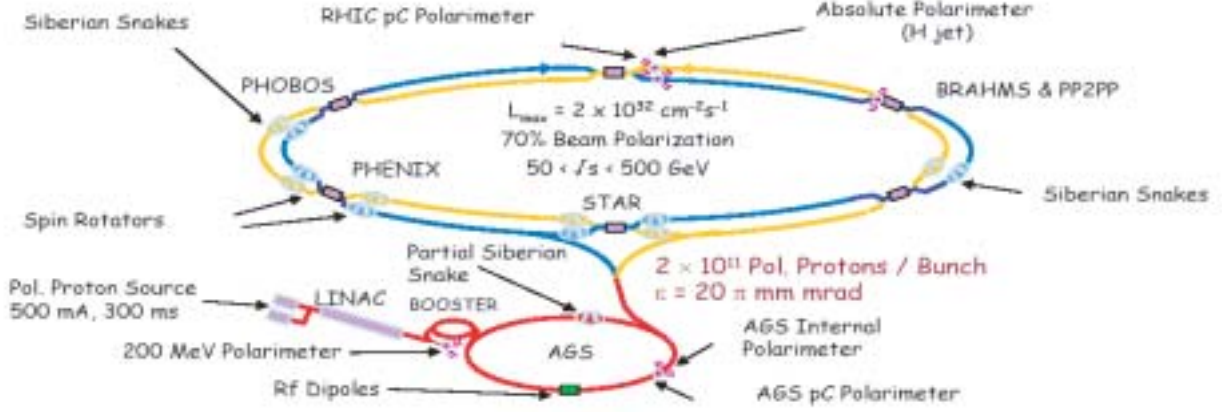


Figure 1.3: The layout of the RHIC Spin complex.

$$N_{\downarrow\uparrow}(t) = \mathcal{L} \frac{d\sigma}{dt} \{1 - A_N(P_1 - P_2) \cos \phi - A_{NN} P_1 P_2 \cos^2 \phi\} \quad (1.11)$$

where \mathcal{L} is the luminosity, P_1 and P_2 respectively refer to the degree of beam polarization for the first and the second beams and ϕ is the azimuthal angle between the normal to the scattering plane and the polarization direction. We then can express the double-spin asymmetry parameter in terms of the quantities above as:

$$A_{NN} = \frac{1}{P_1 P_2 \cos^2 \phi} \frac{N_{\uparrow\uparrow} + N_{\downarrow\downarrow} - N_{\uparrow\downarrow} - N_{\downarrow\uparrow}}{N_{\uparrow\uparrow} + N_{\downarrow\downarrow} + N_{\uparrow\downarrow} + N_{\downarrow\uparrow}}. \quad (1.12)$$

And for the analyzing power, we have:

$$A_N = \frac{1}{P_1 \cos \phi} \frac{N_{\uparrow\uparrow} - N_{\downarrow\downarrow} + N_{\uparrow\downarrow} - N_{\downarrow\uparrow}}{N_{\uparrow\uparrow} + N_{\downarrow\downarrow} + N_{\uparrow\downarrow} + N_{\downarrow\uparrow}},$$

$$A_N = \frac{1}{P_2 \cos \phi} \frac{N_{\uparrow\uparrow} - N_{\downarrow\downarrow} - N_{\uparrow\downarrow} + N_{\downarrow\uparrow}}{N_{\uparrow\uparrow} + N_{\downarrow\downarrow} + N_{\uparrow\downarrow} + N_{\downarrow\uparrow}}. \quad (1.13)$$

It is apparent from these expressions that event rate asymmetries are dominantly in the horizontal azimuth for a vertical beam polarization. Furthermore, the acceptance as a function of t cancels in the expressions for A_N and A_{NN} . Figure 1.3 shows the RHIC Spin complex, including the 2 o'clock IP where this experiment is currently installed.

It has been shown [36] that the asymmetry A_{NN} is sensitive to the contribution from Odderon exchange. This is shown in Fig. 1.4 where curves for A_{NN} are given for three cases of different Pomeron and Odderon contributions. The Odderon should be detectable if the effect has the size presented here.

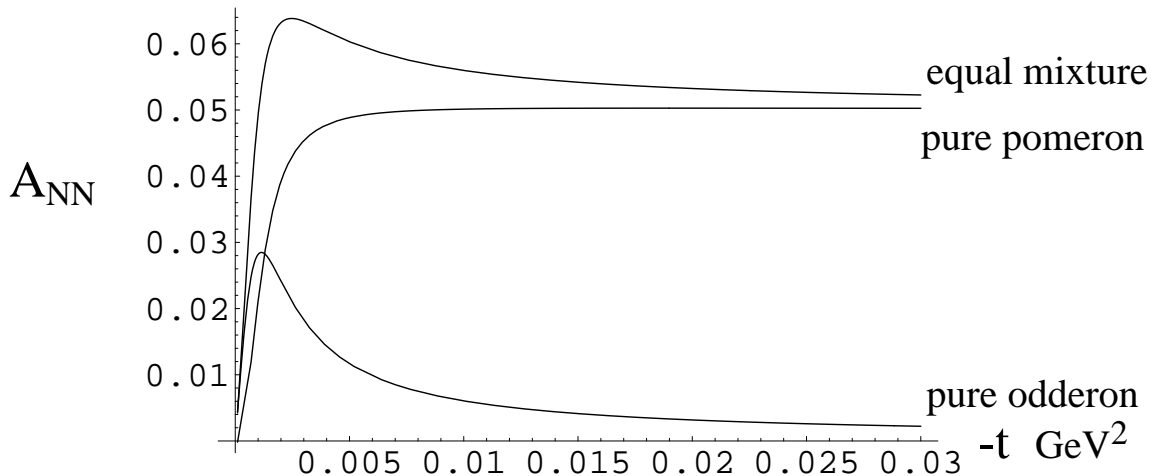


Figure 1.4: This illustrates the enhancement of the Odderon contribution to A_{NN} due to interference with the one-photon exchange. The three curves correspond to $\phi_2/\phi_+ = 0.05i$ (pure Odderon), $\phi_2/\phi_+ = 0.05$ (pure Pomeron) and $\phi_2/\phi_+ = 0.05(1+i)$ (equal mixture). The “pure Odderon” curve is typical of the level of sensitivity expected for this experiment [36].

In addition, the Odderon could show in the dip region of elastic scattering of pp and $p\bar{p}$. Spin dependent asymmetries depend on various real and imaginary parts of products of amplitudes and so the Odderon can dominate some asymmetries to which the Pomeron cannot contribute.

1.3 Unpolarized Elastic Scattering at Small $|t|$

The process of elastic scattering seems most elementary but also is most challenging in terms of theory and calculation. The special role of the elastic channel at high energies is evident from the fact that it contributes as much as 20% to the total cross section. This, coupled with the importance of understanding the diffraction process, not only as the shadow of the many inelastic channels present at high energies, but also in terms of basic concepts related to QCD, has made nucleon-nucleon elastic scattering one of the most studied reactions in high energy physics.

From general considerations of unitarity and analyticity, the difference in the total pp and $p\bar{p}$ cross section is predicted to converge to zero at large values of s ,

$$\frac{\sigma_{tot}(p\bar{p})}{\sigma_{tot}(pp)} \rightarrow 1, \quad (1.14)$$

and the rate at which the pp total cross section rises is limited by the Froissart bound,

$$\sigma_{tot}(s) < \frac{1}{m_\pi^2} \log^2 s. \quad (1.15)$$

The most clear-cut implication of the existence of the Odderon is that it would lead to asymptotically different amplitudes for the scattering of a particle and its anti-particle off the same target. This means that the total cross sections and the differential cross sections for, say, pp and $\bar{p}p$ scattering at high energy will remain different as \sqrt{s} , the total center-of-mass energy, increases; while in the absence of an Odderon they would become the same, roughly as $1/\sqrt{s}$. With pp2pp, a decisive test of this feature becomes possible because of the existence of data at the same energy in $\bar{p}p$ scattering. There are suggestions that the Odderon might be important because the difference between the pp and $\bar{p}p$ differential cross sections in the dip region appears to persist as the energy grows. At the same time fits to σ_{tot} and ρ , the ratio of real to imaginary parts of the forward, helicity-diagonal amplitudes, over a wide energy range for both pp and $\bar{p}p$ leave little room for the Odderon at $t = 0$ [37, 38].

As the summary of elastic scattering measurements and phenomenological models is given in [39], we shall mention only a few open questions here.

By using a perturbative approach, the accepted theory of strong interactions, Quantum Chromo Dynamics (QCD), has been very successful in describing hadronic interactions at large four-momentum-transfer squared $|t|$. For small $|t|$ values of elastic scattering, the theory has not been as successful. This is the regime of soft hadronic interactions where phenomenological models, constrained by asymptotic theorems, are used to explain the nature of the hadronic interaction.

The elastic scattering of protons is described by a scattering amplitude which has two components: the electromagnetic part, described by the well-known Coulomb amplitude f_c , and the hadronic part, described by the hadronic amplitude f_h . The amplitudes are a function of cms energy \sqrt{s} and four-momentum-transfer squared $|t|$. The differential elastic pp cross section can be expressed as a square of the scattering amplitude:

$$\frac{d\sigma_{el}}{dt} = \pi |f_c + f_h|^2. \quad (1.16)$$

The spin independent hadronic amplitude f_h is usually parameterized as:

$$f_h = \left(\frac{\sigma_{tot}}{4\pi} \right) (\rho + i) \exp\left(-\frac{1}{2}b|t|\right). \quad (1.17)$$

The quantity ρ is the ratio of the real to imaginary part of the nuclear amplitude at $|t| = 0$ and is related to the high-energy behavior of the total cross section via dispersion relations. This means that ρ is related to the behavior of the total cross section σ_{tot} at higher energies. The Coulomb amplitude f_c is given by:

$$f_c = -\frac{2\alpha G^2(t)}{|t|} \exp(i\alpha\phi), \quad (1.18)$$

where α is the fine structure constant, $G(t)$, is the proton electromagnetic form factor, and ϕ is the Coulomb phase, which is:

$$\phi = \ln \left(\frac{0.08}{|t|} \right) - 0.577. \quad (1.19)$$

The total cross section is related to the differential elastic cross section by the optical theorem:

$$\sigma_{tot}^2 = \left(\frac{16\pi (\hbar c)^2}{1 + \rho^2} \right) \frac{d\sigma_{el}}{dt} \Big|_{t=0}. \quad (1.20)$$

The dependence of the differential elastic cross section $d\sigma/dt$ on $|t|$ can be divided into three regions: the Coulomb region, the CNI region, and the hadronic region. At small $|t|$, the Coulomb term dominates, and $d\sigma/dt$ has a $(1/t^2)$ dependence. As $|t|$ increases, the interference between the Coulomb and hadronic contributions becomes maximal. Finally, the hadronic contribution dominates, and $d\sigma/dt$ falls off exponentially. The present status of σ_{tot} , ρ , b measurements in pp and $p\bar{p}$ collisions is shown in figures 1.5, 1.6, and 1.7, respectively [40].

In order to determine ρ , one needs to be able to make measurements in the small $|t|$ region. The scale is set by the $|t|$ value where Coulomb and hadronic amplitudes are equal. At $\sqrt{s} = 200$ GeV, this occurs at $|t| \simeq 3 \times 10^{-3}(\text{GeV}/c)^2$, and corresponds to a scattering angle of 0.54 mrad.

Since the Coulomb amplitude is known absolutely, the measurement at very small $|t|$ gives a direct determination of the machine's luminosity and, consequently, the absolute normalization of the hadronic amplitude. As a result, the parameters of the elastic cross section can be determined without requiring an independent measurement of the luminosity or the total cross section.

The pp total cross sections measured at Serpukhov and the Intersecting Storage Rings (ISR) at CERN in the 1970s were found to rise with energy. Before this discovery, it was generally accepted that the total cross sections for both pp and $p\bar{p}$ would decrease as a function of cms energy and converge to a common constant value. The $\ln^2 s$ behavior versus $\ln s$ behavior of the rise of σ_{tot} is still an important topic for investigation.

Among other questions to be explained are the rise of σ_{el}/σ_{tot} for $p\bar{p}$ between ISR and $Spp\bar{S}$ energies, and the existence of a dip in $d\sigma_{el}/dt$ at low energies, which is more pronounced in pp than in $p\bar{p}$ interactions, and its plateau-like shape at the $Spp\bar{S}$ energies.

We intend to make a precision measurement of the energy dependence of the pp total cross section, σ_{tot} , in an uncovered domain of energy, $60 \leq \sqrt{s} \leq 500$ GeV, to be able to make a quantitative comparison with $\sigma_{tot}(p\bar{p})$. In such a way one obtains knowledge about the very important difference $\Delta\sigma = \sigma_{tot}(pp) - \sigma_{tot}(p\bar{p})$, which is critical in distinguishing theoretical models. In the classical Pomeron model, it must go to zero with increasing \sqrt{s} , while other models do not exclude a plateau, or its growth with \sqrt{s} .

1.4 Scattering at Medium Momentum Transfer

Elastic scattering away from the very forward region provides important information on the dynamics of high-energy collisions. The most complete set of proton-proton scattering

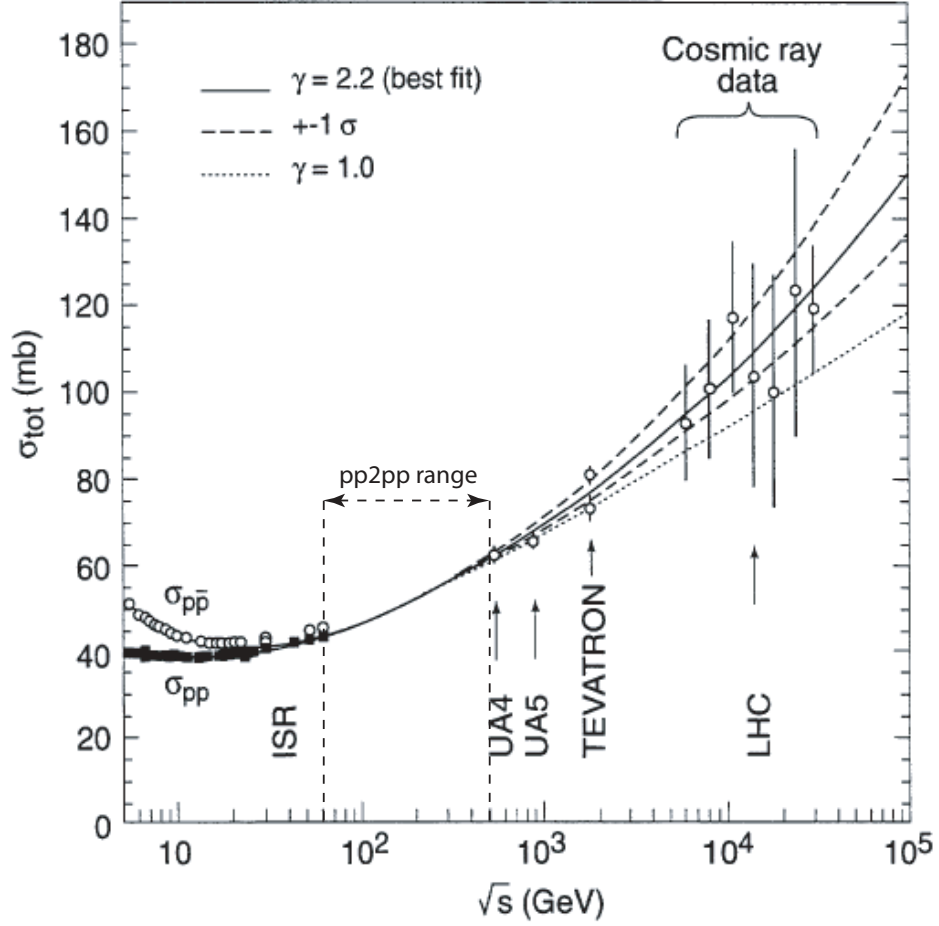


Figure 1.5: The pp and $p\bar{p}$ total cross section σ_{tot} as a function of cms energy [40].

measurements are from the CERN ISR [41], which cover the energy interval from $\sqrt{s} = 23$ GeV up to $\sqrt{s} = 62$ GeV.

These data exhibit a forward diffraction peak with an almost exponential shape which shrinks with energy. A prominent feature is the dip-bump structure at $|t| \simeq 1$ $(\text{GeV}/c)^2$, which is naturally described in the diffraction models. It was in fact predicted by the “geometrical model” of Yang and collaborators, and it is well described in the “impact picture” of Bourrely *et al.* [42] and in the “multiple diffraction model” of Glauber [43]. These models also predict the emergence at higher energy of a more complex structure with secondary maxima and minima that asymptotically become similar in shape to the classical Fraunhofer diffraction by an opaque disk.

In the Regge approach, the observed dip-bump structure can be reproduced if one adopts the procedure of “eikonalization”, where the standard Regge amplitude is treated as a Born approximation [44]. At high-energy, only the Pomeron singularity is relevant. The full

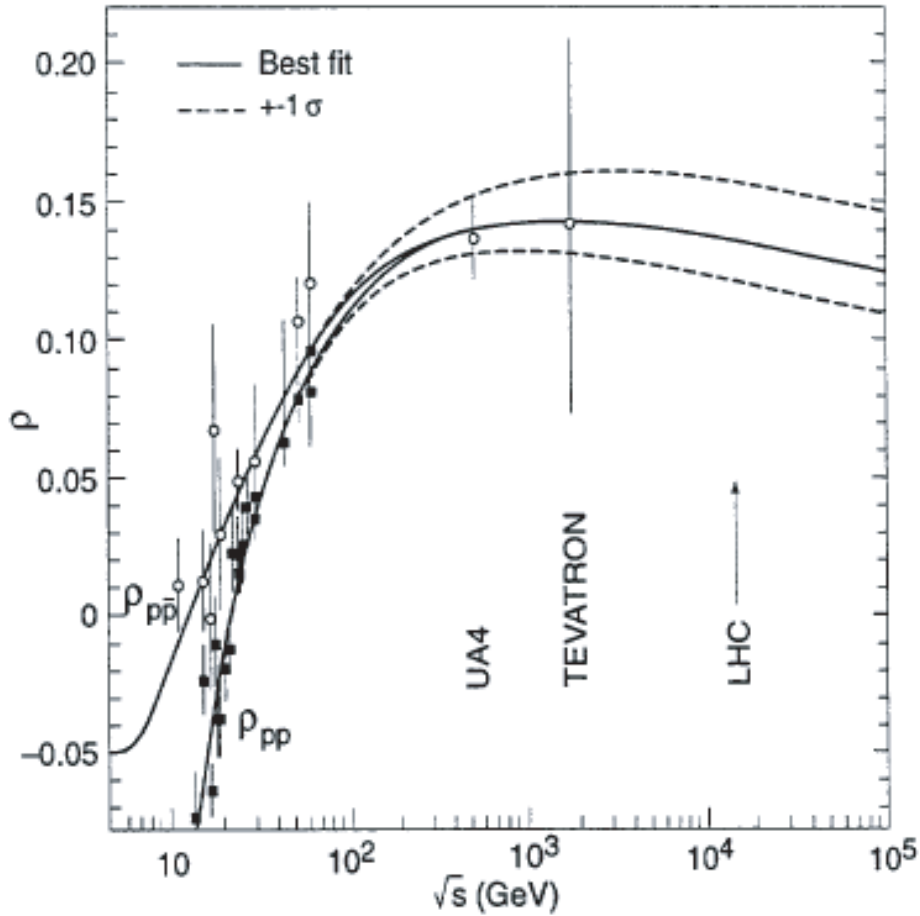


Figure 1.6: The ρ parameter for pp and $p\bar{p}$ elastic scattering as a function of cms energy [40].

amplitude will then be made up of the single Pomeron exchange which dominates at low $|t|$, double Pomeron exchange which becomes effective at larger values of $|t|$, and so on.

The observed structure at $|t| \simeq 1$ $(\text{GeV}/c)^2$ results from the interference of single and double Pomeron exchange [45]. In the specific model of Desgrolard *et al.* [46], a second structure at $|t| \simeq 3.5$ $(\text{GeV}/c)^2$ is predicted to appear already at the RHIC cms energy of 500 GeV.

New experimental information on the region of the diffraction minimum was provided by the proton-antiproton measurements [47] at $\sqrt{s} = 53$ GeV, which are shown in Fig. 1.8 together with the earlier proton-proton data at the same cms energy. In spite of the limited statistics, these data indicate that only a shallow dip is present in $p\bar{p}$ scattering. The difference between the pp and the $p\bar{p}$ channels is explained [48] as due to the presence of the three-gluon-exchange process. The three-gluon amplitude has a different sign for pp and for $p\bar{p}$, and its interference with the other amplitudes produces a dip in pp , but no dip in $p\bar{p}$.

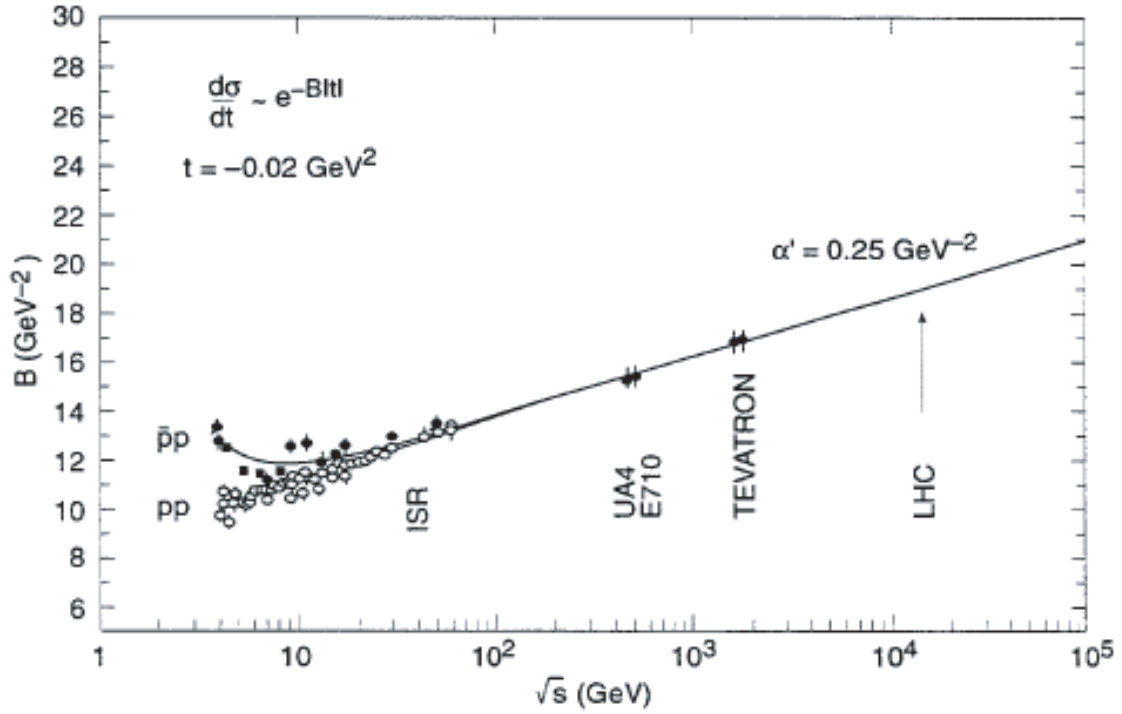


Figure 1.7: The nuclear slope b for pp and $p\bar{p}$ elastic scattering as a function of cms energy [40].

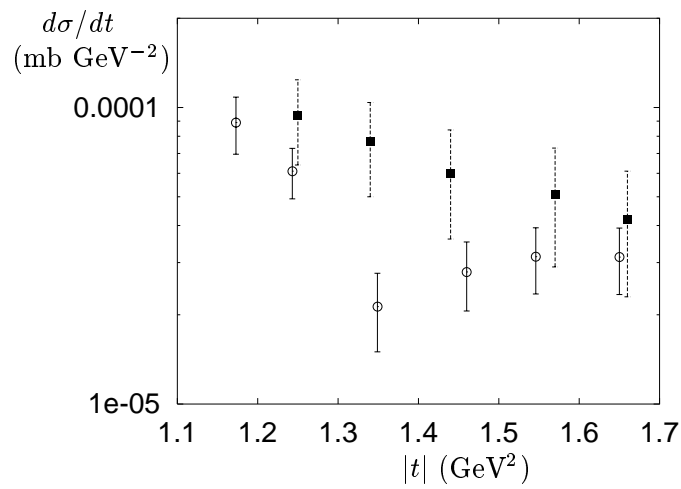


Figure 1.8: The results on pp and $p\bar{p}$ elastic scattering at $\sqrt{s} = 53 \text{ GeV}$.

This feature is expected to be, at least qualitatively, independent of energy.

The proton-antiproton measurements at the CERN $Spp\bar{p}S$ collider have confirmed the expectation that no dip is present in this channel. Only a break followed by a shoulder is observed in the UA4 data [49, 50] at $\sqrt{s} = 546$ and 630 GeV. The Tevatron data at 1.8 TeV from the E710 and CDF collaborations [51] clearly show the persistent shrinking of the diffraction peak with energy, but, unfortunately, do not extend far enough to cover the region of the minimum.

The shoulder in the $Spp\bar{p}S$ collider data is more than one order of magnitude higher than the second maximum seen at the ISR energies. This is well described by the diffraction models and by eikonized Regge models.

The RHIC machine operating in the proton-proton mode offers unique possibilities to investigate elastic scattering further in the region of the diffractive structure and at larger momentum-transfer for \sqrt{s} range 60 to 500 GeV.

Accurate data on the region of the structure provide the opportunity for a direct comparison with the existing $p\bar{p}$ data from the $Spp\bar{p}S$ collider, which are at essentially the same energy, thus probing the theory of the interference of the three-gluon diagram.

The setup of this experiment makes possible a study of scattering at medium momentum transfer, up to $|t| \simeq 1.3(\text{GeV}/c)^2$. As apparent from the previous discussion, the basic question to be addressed is if a new diffraction-like structure will emerge in this $|t|$ region, or will the $|t|$ distribution be smooth and energy independent, controlled by a single QCD diagram?

It is also important to investigate the behavior of the analyzing power A_N at RHIC energies especially in the dip region, where a pronounced structure was found at fixed-target experiments.

Chapter 2

Accomplishments to Date of pp2pp

We review here the equipment that has been built, installed, commissioned and used during two short data taking runs. Later we will review the experimental technique that used this equipment and then describe the results of the 30 hours engineering run in 2002, which has been submitted for publication and the projected results from our short two day data taking run in 2003.

2.1 Existing pp2pp Equipment

Two sets of Roman Pot (RP) stations have been built and installed at the 57 m and 60 m distance, on both sides, relative to the interaction point (IP), shown in Fig. 2.1. We installed the experiment in the 2 o'clock area, and, since our detectors were placed away from the interaction point, they do not interfere with the BRAHMS experiment at the same IP. After scraping of the beam, to reduce the emittance, we were able to approach to within 14 mm of the beam.

The RP stations have been fully instrumented with the silicon strip detectors and a trigger scintillator counter. There were two x and two y planes of detectors for each RP. The silicon strip detector had a strip pitch of 0.1 mm. More details concerning the strip detectors are described in the next section. Behind the strip detectors were the scintillation counters which were 8 mm thick and 80×50 mm² in area and were viewed by two photomultiplier tubes (PMT). The two PMT signals were in a logical OR in the trigger to produce a counter efficiency of greater than 99% and independent of position of the hit.

The trigger system was designed, installed and fully commissioned in the 2002 engineering run along with the data acquisition system. The logic used was an OR of the two PMTs in any pot and then a coincidence with an appropriate pot on both sides of the intersection region. That signal was put into coincidence with a beam crossing signal. It yielded a clean signal of elastic events. In addition, a set of scintillation counters was installed in the IP region to measure a fraction of inelastic scattering events. They were used for luminosity monitoring.



Figure 2.1: The two Roman Pot stations on one side of the IP.

2.2 Overview of the Experimental Technique

2.2.1 Transport Theory

Among the measurements that we had proposed to carry out was the cross section and diffraction slopes at 200 GeV.

For small $|t|$ measurements, we used the accelerator lattice as an analyzer. We found a solution to the accelerator lattice setup that allows the measurement of σ_{tot} , and b in the forward scattering region with small errors at a position roughly 57 m away from the interacting region. The method of determining that point is described below. Special beam scraping was required for the run to allow detection of scattered protons as close to the beam as possible.

The two protons collide at the IP in a local coordinate system at a vertical distance y^* from the reference orbit and scatter with an angle θ_y^* . The scattered particles then pass through various magnetic lenses in the insertion section of the machine lattice until they reach the detector, which measures the positions of the scattered particles with respect to the reference orbit.

In order to be able to measure the scattering angle of the protons, their scattering angle has to be larger than the angular spread of the beam $\sigma_{\theta_y^*}$ at the collision point:

$$\sigma_{\theta_y^*} = \sqrt{\frac{\epsilon}{6\pi\beta^*}}, \quad (2.1)$$

where ϵ is the 95% normalized emittance and β^* is the betatron function at the IP. Thus, a large betatron function at the IP is required to minimize the angular spread of the beam.

The magnitude of the betatron function β^* determines also the size of the beam spot σ_y^* , which is given by:

$$\sigma_y^* = \sqrt{\frac{\epsilon\beta^*}{6\pi}}. \quad (2.2)$$

Since the scattered protons follow trajectories determined by the lattice of the accelerator, the known parameters of the accelerator lattice can be used to calculate the deflection y^* and the scattering angle θ_y^* at the interaction point, knowing the deflection y and the angle θ_y at the detector. At a point where the phase advance from the interaction point is Ψ and the betatron function is β , y is given by [52]:

$$y = \sqrt{\frac{\beta}{\beta^*}}[\cos \Psi + \alpha^* \sin \Psi]y^* + \sqrt{(\beta\beta^*)} \sin \Psi \theta_y^* \quad (2.3)$$

where α^* is the derivative of the betatron function β^* at the interaction point. We have considered a lattice configuration such that α^* is very close to zero.

Equation 2.3 can be rewritten as:

$$y = a_{11}y^* + L_{eff}\theta_y^* \quad (2.4)$$

where

$$a_{11} = \sqrt{\left(\frac{\beta}{\beta^*}\right)}[\cos \Psi + \alpha^* \sin \Psi] \quad , \quad L_{eff} = \sqrt{\beta^*\beta} \sin \Psi. \quad (2.5)$$

The optimum condition for the experiment is to have $a_{11} = 0$ and L_{eff} as large as possible, since the answer is then independent of the coordinate at the IP in the transverse plane of the accelerator and “large displacements” at the detection point are obtained for small scattering angles. This is achieved when Ψ is an odd multiple of $\pi/2$. The expression for the y coordinate at the detection point then simplifies to:

$$y = L_{eff}\theta_y^*. \quad (2.6)$$

Therefore, if the detector is located at a point where the phase advance is an odd multiple of $\pi/2$, then the scattering angle is determined just from the measurement of the displacement alone. With the above condition satisfied, rays that are parallel to each other at the interaction point are focused onto a single point at the detector, commonly called “parallel to point focusing.”

Another question, related to the optimization of the accelerator setup, is the smallest measurable four-momentum-transfer squared t_{min} . The goal is to achieve t_{min} as small as possible. The t_{min} is determined by the smallest scattering angle measured θ_{min}^* , which, using Eqn. 2.6, is given by:

$$\theta_{min}^* = \frac{d_{min}}{L_{eff}}, \quad (2.7)$$

The minimum distance of the approach to the beam, d_{min} , can be expressed in terms of the beam size at the detector position and the “dead space of the detector” d_0 :

$$d_{min} = k\sigma_y + d_0, \quad (2.8)$$

where k is a machine dependent constant, which is optimized by beam scraping, and σ_y is the beam size at the detection point. Assuming d_0 is small, the t_{min} is then:

$$|t_{min}| \approx \frac{k^2\epsilon p^2}{\beta^*}. \quad (2.9)$$

We can see that the smallest t_{min} is reached by having β^* as large as possible and by reducing the k -factor and the emittance, in other words by optimizing the beam scraping.

2.2.2 Actual Beam Transport

The geometry of the outgoing beam transport at the IP2 is displayed in Fig. 2.2. Proton beams travel from left to right in this lattice along a central design trajectory. The Roman Pot stations (RP) in the Q3–4 warm straight detect protons that have elastically scattered at IP2, limited by the Q1–3 quadrupole apertures and detector acceptance. It is important to know the beam transport of these scattered protons between IP2 and the detectors to understand systematics in the reconstruction of scattering data.

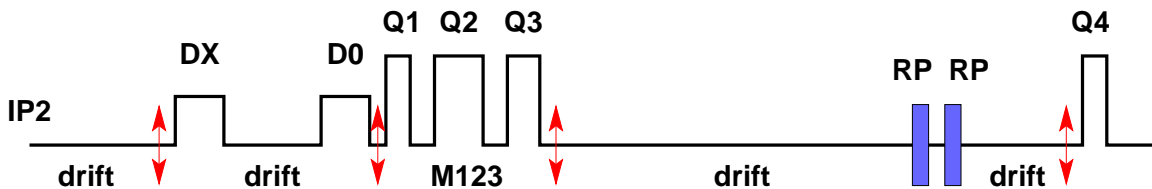


Figure 2.2: pp2pp IP2 lattice layout. Drift transport is trivial when the geometry is known. Knowledge of the off-axis triplet transport **M123** and DX/D0 multipole fields is then required to obtain scattered proton transport to the few percent level.

Primary beam measurements cannot be used to directly measure the off-axis near-aperture quadrupole fields and scattered beam transport, due to the likelihood of a superconducting magnet quench. Primary beam transport is instead measured on the design orbit, confirming magnet settings and knowledge of local imperfections such as triplet quadrupole roll angles. This measurement is performed by exciting the beam with tunemeter kickers or an AC dipole, and using local dual-plane BPMs (shown as double-headed arrows in Fig. 2.2), and confirms local phase advances and beta functions with systematics of a few percent and randoms of less than a percent. This measurement is not sensitive to systematics in BPM gains or offsets.

Another beta function measurement is performed at each IP quadrupole, varying its individual focusing strength over several points by a few percent and measuring the corresponding tune change with the PLL tunemeter: $\langle\beta(s)\rangle = -4\pi \Delta\nu/\Delta KL(s)$. This is a dedicated measurement because such tune changes can lead to depolarization and even beam loss. It is sensitive to systematic errors in the PLL system, but during the FY03 run this measurement was consistent with the excited beam measurements to a few percent.

These phase and beta function measurements are then compared to a model based on measured magnet currents, using measured transfer functions from the RHIC magnet database, measured RHIC survey offsets, and measured triplet roll angles. Agreement is confirmation that base optics are correct. These base optics are then extrapolated to off-axis field maps using triplet field components up to decapole as measured for the specific RHIC triplet quadrupoles of IP2. These extrapolations are conservatively good to 1% at a position as close as 1 mm to the coil aperture [53]. They are expected to provide systematic trajectory-dependent corrections to pp2pp beam transport at the level of a few percent.

2.2.3 Measurement of the Beam Angle and Position at the IP

The geometry of the IP2 between the DX separation magnets is shown in Fig. 2.3. Beam trajectories through this straight section are measured with two DX BPMs, each attached to the IP-side of the corresponding DX magnet cryostat. The beam collision point is where these two trajectories cross. The vertex can be compared to the elastic scattering vertex distribution, and vertex corrections can be applied to further eliminate beam transport systematics.

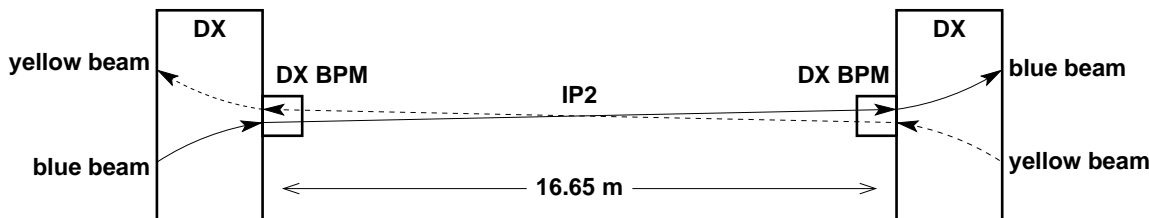


Figure 2.3: Overhead view of IP2 between the DX magnets (not to scale), showing beam trajectories and locations of the DX BPMs g1-bx and g2-bx. A small symmetric crossing angle has been added for clarity.

For proper vertex corrections, the measured vertex must be in the same reference frame as the roman pot survey. Calculation of the vertex from measured DX beam centroid positions have several systematics that must be removed:

- Survey offset: The DX BPMs are attached directly to the flanges of the DX magnet cryostat, and were surveyed on January 10, 2001. These offsets are the same for both rings since the DX BPMs see both beams.

- Electronics gain: DX BPM electronics are calibrated with onboard pulsers several times per run, but have channel-specific gain and offset calibration errors that range up to several mm. These errors are gain-setting dependent. These offsets can be measured by comparing position calculated from raw BPM signals to position calculated by the acquisition electronics.

Some systematics can be constrained with the knowledge that the beams are colliding at the time of measurement. Work is underway to improve the DX BPM system timing, and directly measure raw signals and electronics gain offsets before and during the next run.

2.2.4 Silicon Strip Detector

Thirty two silicon strip detectors, with associated front end electronics, were used in pp2pp and had greater than 99.5% of working channels. Five spares with similar performance exist. Additionally, three spares are under repair and can be expected to achieve the same level of performance.

The silicon detectors are 400 μm thick, AC-coupled, single-sided strip detectors with an approximate pitch of 100 μm . They feature p^+ strips on n-type silicon bulk. Each p^+ strip is terminated with a 2 M Ω polysilicon bias resistor. The detectors feature a double-metal fan-in from the 100 μm strip pitch to a 48 μm pitch at the detector edge. This permits connection to readout chips that are designed for the more commonly used 50 μm pitch detectors. There are two types of the detectors, an x-view detector with vertical strips and a y-view detector with horizontal strips. Each type is approximately $7.5 \times 4.7 \text{ cm}^2$ in size. The detectors were manufactured by Hamamatsu Photonics.

The detectors are read by the SVXIIE [54] readout chip that was originally designed for the D0 experiment at Fermilab. The SVXIIE is designed in a 0.1 μm CMOS process and has 128 input channels. Each channel features a charge integrator followed by an analog pipeline capable of storing signals from the previous 32 bunch crossings. The SVXIIE features a Wilkenson-type ADC for simultaneous digitization of all channels upon receipt of a trigger. Upon readout the SVXIIE outputs first a programmable chip id number followed by alternating 8-bit digitized data and channel number for all 128 channels. An option known as "sparsification" or "zero suppression" exists for the SVXIIE to output only those channels whose data exceed a preset threshold.

The detectors and readout chips are mounted on custom printed circuit boards (detector boards) that provide differential digital communication between the SVXIIE chips and a control and readout module. Additionally, a microprocessor controlled power board plugs into each detector board to provide several voltages that can be enabled in the proper sequence required by the SVXIIE. Each Roman pot contains an assembly of two x-view detectors, two y-view detectors, and a trigger scintillator. A photograph of an assembled package is shown in Fig. 2.4.

A control and readout module designed for pp2pp is the SVX Sequencer and Memory Module (SSMM). This module is a custom VME board that communicates with the detector board and generates control and clocking signals to run the SVXIIE chips. Additionally, the SSMM contains sufficient memory to store several events of silicon data arriving from one

Roman Pot. It has the additional feature that it can simultaneously read data from the detector boards while writing out data over the VME backplane to maximize event rate. In the configuration used in pp2pp this resulted in a maximum data rate of about 400 Hz.



Figure 2.4: Assembled detector package on survey bench without trigger scintillator.

2.3 The Engineering Run in 2002

Part of our experiment was installed for the engineering run in 2002. The layout of the experiment is shown in Fig. 2.5. The Roman Pots located at 57 m were fully instrumented with silicon detectors. The average silicon detector plane efficiency for arm A was 0.97. The triggering system, the data acquisition and the silicon strip detectors were debugged parasitically.

During a dedicated engineering of two days at the end of the RHIC pp running, the beam was scraped, the emittance lowered and the RP's were inserted close to the beam. Data were taken for about 14 hours.

In the analysis of the data, elastic events are identified by requiring the collinearity between two outgoing protons, hence it requires the simultaneous detection of the scattered protons. The collinearity of elastic events implies that the two coordinates obtained from the silicon detectors on either side of the interaction point are correlated. This correlation is shown for the y coordinates from arm A in Fig. 2.6. The elastic signal was clean and a region of flat acceptance was obtained for $0.010 \leq |t| \leq 0.019$ $(\text{GeV}/c)^2$ after constraining the ϕ range to $45^\circ \leq \phi \leq 135^\circ$, shown in Fig. 2.6.

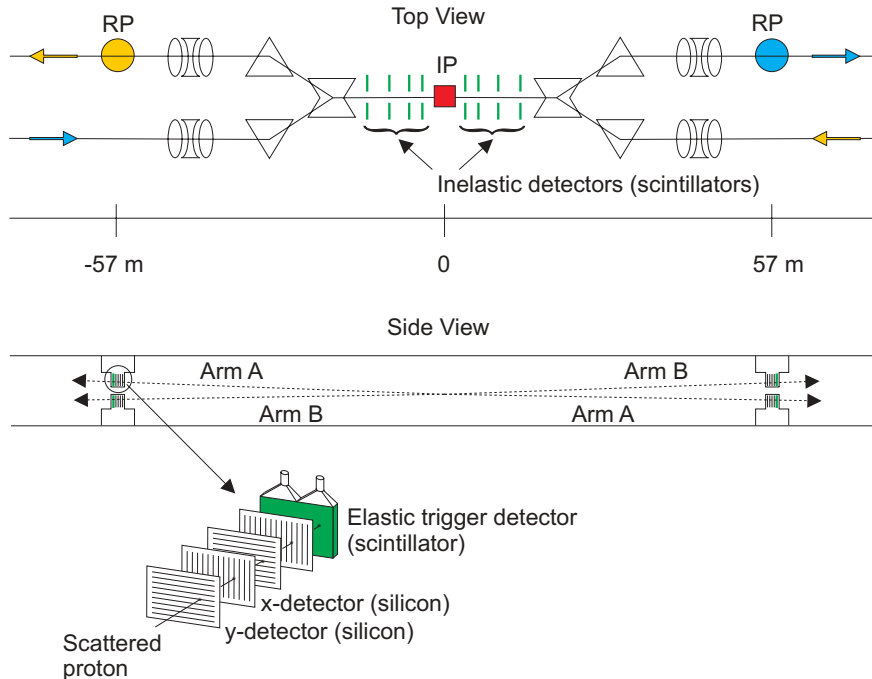


Figure 2.5: Layout of the pp2pp experiment for the engineering run. Note the detector pairs RP and RP' lie in different RHIC rings. Scattering is detected in either one of two arms: Arm A is formed from the upper half of RP' and the lower half of RP. Conversely, Arm B is formed from the lower half of RP' and the upper half of RP.

Based on the final selection of 58,511 elastic events we obtained a value of the slope parameter $b = 16.3 \pm 1.6(\text{stat.}) \pm 0.9(\text{sys.}) (\text{GeV}/c)^{-2}$, which is shown in Fig. 2.7 together with the world data on elastic pp and $p\bar{p}$ scattering. This result is about one standard deviation higher than an extrapolation of world data to the energy of this experiment [37], [38], [55]. It agrees well with model predictions [42]. This result has been submitted for publication. See the attached preprint for more details.

We also measured the single spin counting rate asymmetry ε_N over the range of $0.01 \leq |t| \leq 0.02(\text{GeV}/c)^2$ as a function of the azimuth, ϕ . Assuming a beam polarization measurement of $P_{\text{beam}} = 0.24 \pm 0.10$ resulted in an analyzing power of $A_N = 0.033 \pm 0.016$. The result is shown in Fig. 2.7.

2.4 The Data Taking Run in 2003

For the 2003 run, new silicon strip detectors were made and two sets of RP's were instrumented at two sides, 57 m and 60 m from the IP. A two day run was granted. Rather

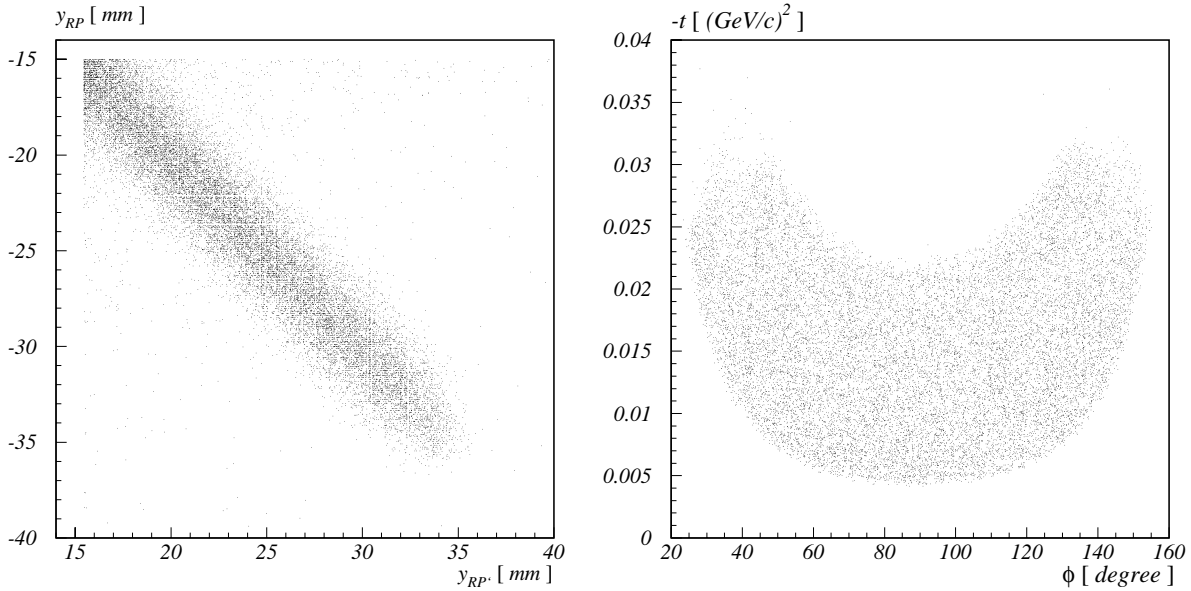


Figure 2.6: Correlation between the y coordinates as measured by the two detectors of arm A for elastic events before cuts being applied. Correlation between t and ϕ for reconstructed events.

than doing extensive scraping to reduce the emittance of the beam, as was done in 2002, we injected a low intensity, low emittance beam from the AGS. The polarization for this run was estimated to be 0.37, in comparison to the previous run, at which the polarization was estimated to be 0.24.

We obtained an order of magnitude more data than in the engineering run. We also had been able to carry out a Van der Meer scan at the end of the run to enable us to make a measurement of the total cross section. During the Van der Meer scan we calculated data related to the signals used in the scan. Using our offline analysis we can make correction for background separately for each of the points in the scan. We estimate to have an error on the luminosity measurement of less than 5%. We also made a series of beam transport measurements during this run and with the second set of RPs we can make a measurement of the local angle. This will enable us to understand the beam transport better and therefore reduce our systematic errors.

From this run we expect to be able to measure the slope parameter to ± 0.35 , the total cross section to about 5% and the raw asymmetry ε_N to 0.001 for a single data point.

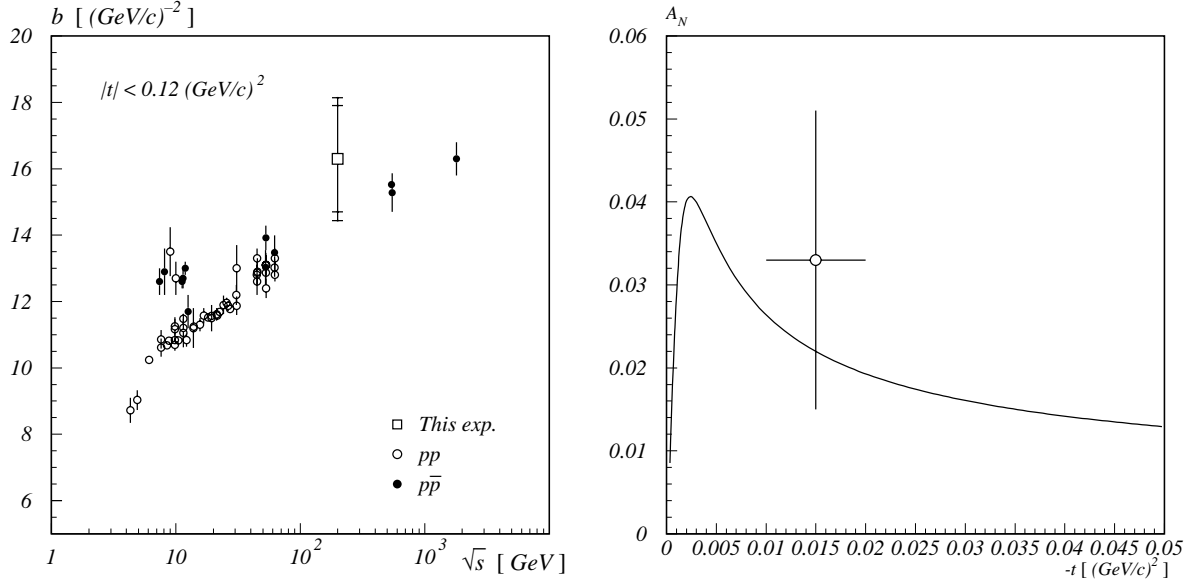


Figure 2.7: The result for the slope parameter b of this experiment compared to the world pp and $p\bar{p}$ data set. The data are drawn from the Durham Database Group (UK). Only statistical errors are shown. The analyzing power without possible contribution of a hadronic spin-flip amplitude to the interference. The data point is a preliminary measurement obtained during the engineering run, the vertical error bar indicates the statistical error, including the uncertainty from the beam polarization measurement, and the horizontal error bar indicates the $|t|$ range of the measurement.

Chapter 3

Proposed Plan for the Experiment

In this chapter we describe what physics can be achieved in three phases of the experiment:

1. Phase 1: Running with the current setup to measure and study the spin dependence of elastic scattering at $\sqrt{s} = 200$ GeV with $\beta^* = 20$ m and $\sqrt{s} = 500$ GeV with $\beta^* = 10$ m. Cost of miscellaneous items for this phase is about \$ 25k. Our request is for three days of data taking at each of the two energies of $\sqrt{s} = 200$ GeV and $\sqrt{s} = 500$ GeV;
2. Phase 2: Running with Roman Pots in the DX-D0 region, we will extend the $|t|$ range at $\sqrt{s} = 200$ GeV to $0.2 (\text{GeV}/c)^2$ and to study the diffractive minimum region and its spin dependence at $\sqrt{s} = 500$ GeV to $1.3 (\text{GeV}/c)^2$. The additional cost of modification of DX-D0 region and new Roman Pot stations, while using the existing detectors, is about \$ 452k. No dedicated running time is required for this phase, because no special conditions are required;
3. Phase 3: Extend the $|t|$ range into the Coulomb region of elastic scattering to make precision measurements, as outlined in the original proposal, of ρ , σ_{tot} , and the spin dependence of $\Delta\sigma_{tot}$. With that setup detailed information of helicity amplitudes at small $|t|$ will shed light on σ_{tot} . Cost of the power supplies for this phase is \$ 362k. We expect two days of time for data taking at each energy plus setup time of the beam optics.

3.1 Phase 1: Running with the current setup

The present experimental setup is suitable for additional measurements in an extended $|t|$ and ϕ range. At $\sqrt{s} = 200$ GeV one can use the capacity of the existing power supplies to run with the accelerator optics of $\beta^* = 20$ m. This tune at $\sqrt{s} = 200$ GeV makes it possible to extend the kinematic coverage to a lower $|t|$ of $0.003 \leq |t| \leq 0.020 (\text{GeV}/c)^2$. The $\beta^* = 20$ m solution, as shown in Table 3.1, also allows the measurement in the horizontal plane and hence makes the ϕ region of maximum analyzing power accessible by rotating one of the

RP stations into the horizontal position. At $\sqrt{s} = 500$ GeV the optics with $\beta^* = 10$ m will be used, allowing measurements up to $|t| \approx 0.12$ (GeV/c)².

The analyzing power has a maximum value of $A_{max} = 0.04$ ($\sqrt{s} = 200$ GeV) at $|t| = 0.0024$ (GeV/c)² and its $|t|$ dependence towards larger values of $|t|$ is sensitive to a possible contribution to the single spin-flip amplitude, ϕ_5 , from the interference between the hadronic spin-flip amplitude with the electromagnetic non-flip amplitude. The calculation, taking only the interference between hadronic non-flip amplitude and electromagnetic spin-flip amplitude into account, leads to a slow decrease with $|t|$, as shown in Fig. 2.7. A fast decrease of A_N with $|t|$ reaching or crossing zero in the same $|t|$ range will be indicative of a large imaginary part of ϕ_5 , while a shift to higher or lower values of A_N at $|t|$ above 0.005 (GeV/c)² will reveal a contribution of the real part of ϕ_5 . The position and value of the maximum A_N is predicted to be not sensitive to the different contributions to ϕ_5 [18]. A precise measurement of the $|t|$ dependence of A_N in the above given $|t|$ range is necessary to disentangle the different contributions to ϕ_5 .

An additional contribution of the hypothetical Odderon to the pp scattering amplitude can be probed by measuring the double spin-flip asymmetry, A_{NN} [36]. As shown in Fig. 1.4, A_{NN} is sensitive to contributions of the real and imaginary parts to the double spin-flip amplitude, ϕ_2 , in the range $0.003 < |t| < 0.010$ (GeV/c)². At a higher value of $|t|$ the difference between a pure Pomeron contribution and an equal mixture of Pomeron and Odderon at the five percent level are hard to distinguish, while a pure Odderon contribution would lead to a very small double spin-flip asymmetry.

The measurement of the differential pp cross section over the extended $|t|$ range will include the region at the lower $|t|$ that is particularly sensitive to ρ . This will make the extraction of ρ and b in a combined fit to the differential cross section possible. No measurement of ρ has been made thus far and the uncertainty in its values is contributing at present a correlation uncertainty to the measurement of b .

Table 3.1: Transport matrix elements in x and y coordinates.

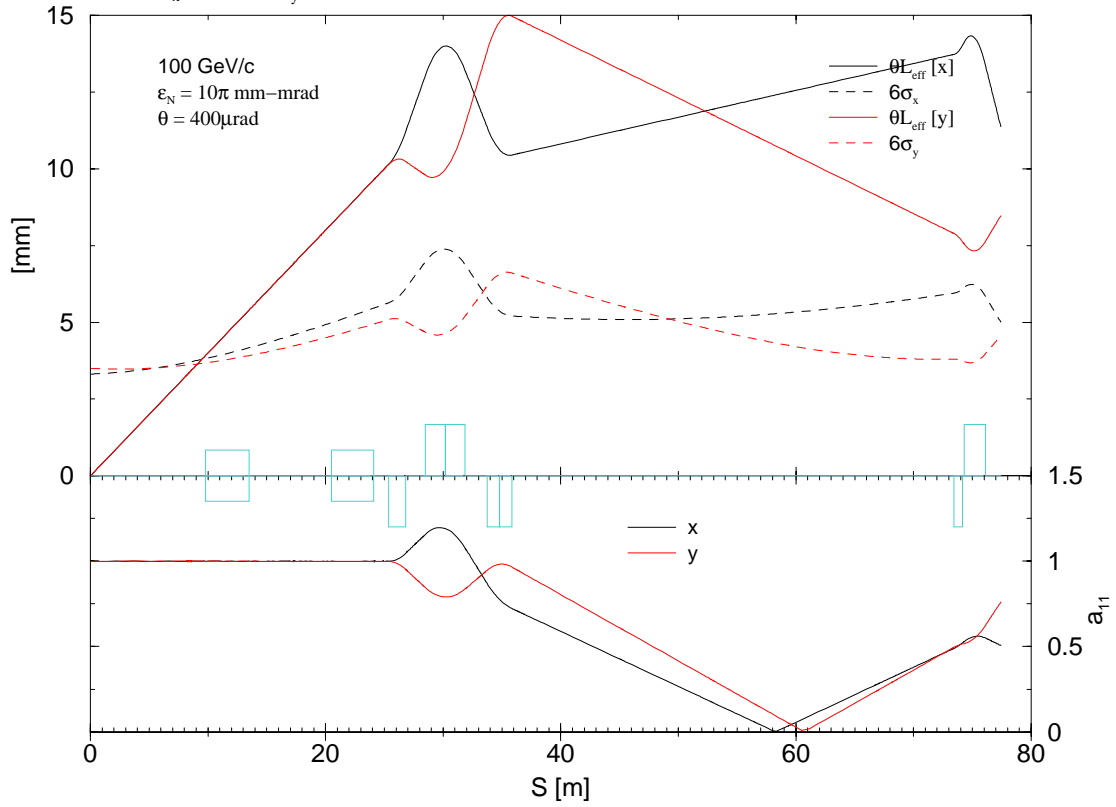
Transport matrix element	Value at 57 m	Value at 60 m
a_{11} in y	0.156	0.044
L_{eff} in y	27.509 m	26.232 m
a_{11} in x	0.051	-0.041
L_{eff} in x	30.613 m	31.306 m

For the accelerator tune with $\beta^* = 20$ m the transport of scattered protons to the Roman Pot stations, located at the 57 m positions, was simulated. The parameters used in the Monte Carlo simulation are listed in Table 3.1. A typical trajectory of a proton scattered at $\theta_x = \theta_y = 400$ μ rad scattering angle, $|t| = 0.003$ (GeV/c)², is shown in Fig. 3.1, where one can see a clear separation of that trajectory from the beam envelope.

The setup time of the β^* to 20 m is estimated by the C-A department to be 12 hours.

RHIC Insertion Functions

$v_x = 28.22$ $v_y = 29.23$ $\beta^* = 20.6297$ FILE = optics/rhbluepp2pp.optics



Time: Mon Mar 24 09:56:35 2003 Last file modify time: Mon Mar 24 09:39:06 2003

Figure 3.1: The RHIC Insertion function for $\beta^*=20$ m

With 20 hours of data taking during one long store six million elastic events can be recorded. With this data sample a statistical error of $\Delta\varepsilon_N = 0.0017$ for each of the six points of the raw counting rate asymmetry in the interval $0.003 < |t| < 0.020$ $(\text{GeV}/c)^2$ can be obtained. The analyzing power is related to the raw asymmetry by $A_N = \frac{\varepsilon_N}{P_{yellow} + P_{blue}}$. Assuming a beam polarization of $P_{yellow} = P_{blue} = 0.4 \pm 0.1$ for each of the two beams would lead to a statistical error of $\Delta A_N = 0.004$ for each of the six data points.

The measurement of the double-spin asymmetry, A_{NN} , depends on the measurement of the relative luminosities, needed for normalization of the four spin-dependent counting rates involved. In addition, the statistical error depends on the square of the beam polarization. With the above assumptions for beam polarization and error, a value of 0.01 for A_{NN} , and six million elastically scattered protons, the error on the double-spin asymmetry was estimated to be $\Delta A_{NN} = 0.03$ for a single data point over the entire $|t|$ range. The expected higher beam polarization and smaller error on the polarization measurement will substantially reduce our conservative estimate of the error on A_{NN} . This would improve the constraint this experiment can place on the Odderon contribution to this asymmetry.

We conclude from our simulations that the suitable $|t|$ interval to fit ρ and b is $0.003 < |t| < 0.02$ $(\text{GeV}/c)^2$. For this amount of data the above described simulation with input parameters of $\sigma_{tot} = 51.5$ mb, emittance $\epsilon = 15\pi \cdot 10^{-6}$ m, gave an error on the slope parameter $\Delta b = 0.3$ $(\text{GeV}/c)^{-2}$ and on the ratio of real to imaginary part of the scattering amplitude $\Delta\rho = 0.01$, which is comparable to the existing measurements of ρ from the pp and $p\bar{p}$ data.

At $\sqrt{s} = 500$ GeV A_N and A_{NN} can be measured with the same errors. However, since the useful absolute $|t|$ interval is $0.025 < |t| < 0.12$ $(\text{GeV}/c)^2$, which is far from the CNI region, one can measure b with $\Delta b \approx 0.3$.

Our request is for three days of data taking at each of the two energies of $\sqrt{s} = 200$ GeV and $\sqrt{s} = 500$ GeV.

3.2 Phase 2: Medium $|t|$ Region

In this medium $|t|$ region, the collinearity condition and the additional momentum analysis, using the DX magnet as a analyzing magnet, will be used to reconstruct elastically scattered protons.

We list in Table 3.2 the relevant parameters of two typical experiments, the experiment by Nagy *et al.* [41] in pp scattering at the CERN ISR using the ‘‘Split Field Magnet’’ and the UA4 experiment [49, 56] at the $Spp\bar{S}$ collider using a system of Roman pots behind the insertion quadrupoles.

In the proton-proton mode at RHIC, the expected normalized emittance, defined at the 95% level, is $\epsilon = 15\pi \cdot 10^{-6}$ m. The size and angular divergence of the beam, the r.m.s. values, are given by Eqn. 2.1 and Eqn. 2.2. At $\sqrt{s} = 500$ GeV and for the betatron function at the crossing point $\beta_x^* = \beta_y^* = 10$ m, the size and angular spread of the beam at the crossing are $\sigma_y = 0.40$ mm and $\sigma_{\theta_y} = 40$ μrad respectively.

The scattered protons will be measured by silicon strip detectors in the Roman pots downstream of the interaction point using the DX magnet to make the momentum analysis.

Table 3.2: Parameters of ISR, UA4, and this experiment.

	ISR	UA4	This Experiment
Energy $cms \sqrt{s}$ (GeV)	23 - 62	546 - 630	60 - 500
Luminosity $cm^{-2}s^{-1}$	few 10^{30}	few 10^{28}	5×10^{30}
Maximum $ t $ (GeV/c) ²	10	$\simeq 2$	$\simeq 1.3$
Momentum resolution $\Delta p/p$	$\simeq 5\%$	$\simeq 0.6\%$	$\simeq 1.5\%$
Momentum-transfer resolution Δt	$\simeq 0.015\sqrt{ t }$	$\simeq 0.06\sqrt{ t }$	$\simeq 0.02\sqrt{ t }$

Since the detectors are placed in the vertical plane, symmetrically above and below the machine plane, the horizontal bending of the DX magnet allows an almost complete decoupling between the measurement of the scattering angle, essentially given by the vertical coordinate, and the measurement of the momentum, obtained from the horizontal coordinate.

In order to implement this solution, the modification of the current vacuum chamber is required. This modification will allow installation of two Roman Pot stations separated by about 3 m and will not impact the operation of the zero degree calorimeters in that location. The design assures that the limiting aperture is due to the opening of the DX magnet. The outline of the Roman Pot stations overlaid on the beam pipe region between the DX and D0 magnets is shown in Fig. 3.2 for both top view and the plan view. They fit well in the space available.

Since no quadrupoles are present in front of the D0 magnets in this region, the beta function at the distance L from the crossing point is:

$$\beta = \beta^* + L^2/\beta^*. \quad (3.1)$$

A Monte Carlo program was used to study the basic features of the system, such as the acceptance and the resolution in the measurement of the momentum and of the momentum-transfer. Size and angular divergence of the beam at the collision region, as derived from the nominal machine parameters, were taken into account. The expected minimum distance of approach of the detector to the beam was calculated according to Eqn. 2.8, with k -factor of 15 and $d_0 = 1.8$ mm and is estimated to be 14 mm. The resulting geometrical acceptance as a function of $|t|$ is shown in Fig. 3.3.

The ultimate momentum-transfer resolution is determined by the actual angular spread of the circulating beams, as given by the machine emittance, and by the beta value at the collision point:

$$\Delta t = 2p\Delta\theta\sqrt{|t|}, \quad (3.2)$$

where the ultimate error on the scattering angle is $\Delta\theta = (1/\sqrt{2})\sigma_{\theta_y}$. Numerically,

$$\Delta t = 1.6 \times 10^{-2}\sqrt{|t|}. \quad (3.3)$$

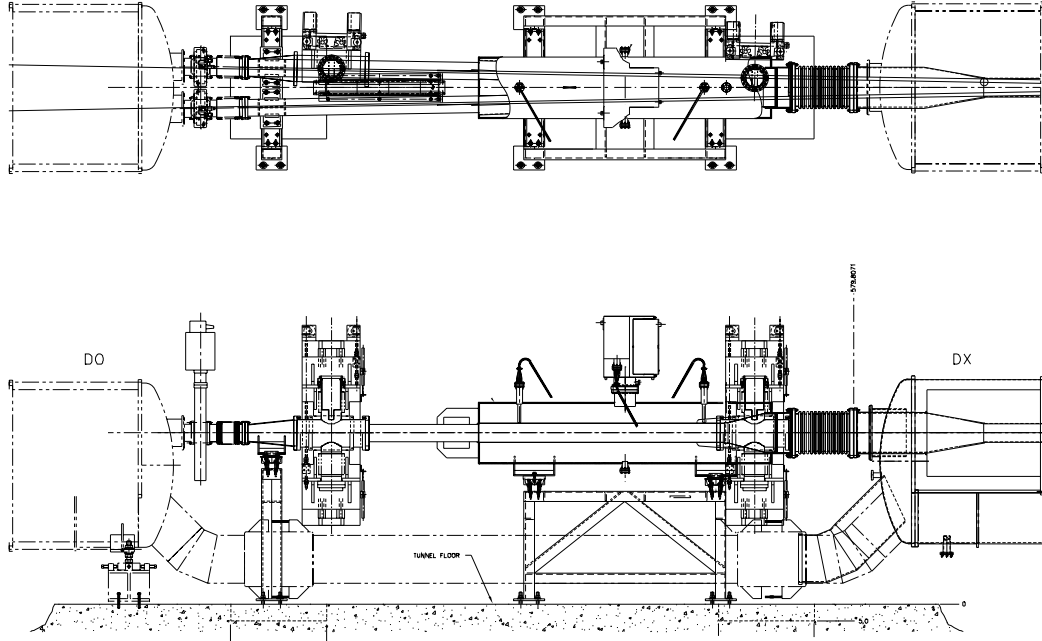


Figure 3.2: Arrangement of the Roman Pots for the medium $|t|$ measurement, two Roman Pots per telescope, spaced by 3 m, positioned between the DX and D0 magnets (top and side view of the setup.)

The actual $|t|$ resolution is somewhat worse because of the effect of the beam size and the resolution of the detectors. In the Monte Carlo simulation, it was derived from the difference between the true value of $|t|$ and the one obtained after reconstruction. Unless specified, the detector resolution was taken to be $30 \mu\text{m}$, the same for both the horizontal and the vertical coordinate.

The expected performance for this proposal is:

- Momentum analysis with $\Delta p/p \leq 1.5\%$; we shall take advantage of the deflection by the dipole magnet DX, which is located at the end of the straight section;
- Reconstruction of the collision point by extrapolating the observed tracks back to the crossing region, with an accuracy sufficient to reject beam-wall interactions;
- Momentum-transfer resolution better than $\Delta t = 0.02 (\text{GeV}/c)^2$ at $|t| = 1 (\text{GeV}/c)^2$;
- The useful momentum-transfer interval is $0.2 < |t| < 1.3 (\text{GeV}/c)^2$;

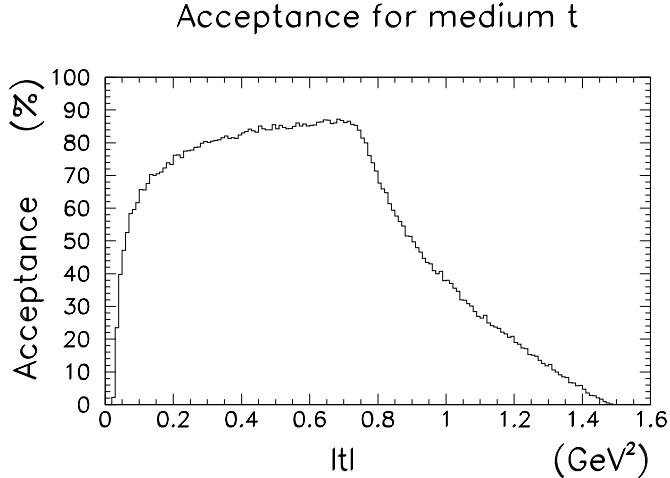


Figure 3.3: Geometrical acceptance as a function of the momentum transfer.

- At $|t| = 1 \text{ (GeV/c)}^2$, the expected cross section is around $10^{-3} \text{ mb (GeV/c)}^2$, and the acceptance of the system is about 0.25. With a luminosity of $5 \times 10^{30} \text{ cm}^{-2}\text{s}^{-1}$, the expected rate is about 5×10^3 elastic events per day in $|t|$ -bin of 0.05 (GeV/c)^2 .

3.3 Phase 3: CNI Region

In this phase, a precision measurement of A_N and A_{NN} will be made over an extended $|t|$ range reaching into the Coulomb region. The ρ value and σ_{tot} will also be measured. To accomplish those goals at $\sqrt{s} = 500 \text{ GeV}$ the RP stations will be moved to a location 70 m from the IP, where parallel to point focusing is realized with $\beta^* = 100 \text{ m}$. The main cost of this phase is due to the additional power supplies, needed for the focusing quadrupoles to provide enough current to obtain the $\beta^* = 100 \text{ m}$ optics and its estimate is detailed in Chapter 4. The event rates are large, so we are requesting three days of running at each energy, $\sqrt{s} = 200 \text{ GeV}$ and 500 GeV .

The luminosity for pp interactions with the special lattice tune will be about $2 \times 10^{28} \text{ cm}^{-2}\text{sec}^{-1}$. The measurement of the elastic cross section $d\sigma/dt$, either in combination with the measurement of the Coulomb scattering amplitude, or with the total cross section allows us to measure the luminosity. It will be useful to compare the measurement of σ_{tot} in the Coulomb region with the Van der Meer scans. As a result a 1% calibration error on the luminosity measurement at RHIC can be achieved.

In the method proposed here, the measured distribution is normalized absolutely by measurement of the Coulomb elastic scattering amplitude $d\sigma_C/dt = 4\pi\alpha^2/t^2 = 2.61 \times 10^{-31}/t^2 \text{ cm}^2 \text{ (GeV/c)}^2$ for very small values of $|t|$ where the Coulomb scattering dominates and $G(t) \simeq 1$. A fit of the full dN/dt -distribution, after acceptance correction and background subtraction, can be done with σ_{tot} , the ρ -parameter, and the nuclear slope b as free

parameters. The luminosity \mathcal{L} at the IP is then simply found from comparison with the actual number of events, after acceptance corrections and background subtraction. However, the Coulomb amplitude dominates only at very small $|t|$. In order to measure the Coulomb amplitude well, one therefore has to measure very close to the beam as described by Eqn. 2.9. Because of the fine segmentation of our silicon strip detector the sharp θ^{-4} rise of the Coulomb scattering cross section at small angle θ can be well measured.

The Coulomb cross section $d\sigma/dt|_{t=t_{min}} \simeq 1.6 \times 10^{-24} \text{ cm}^2/(\text{GeV}/c)^2$, so that at $\mathcal{L} = 2 \times 10^{28} \text{ cm}^{-2}\text{s}^{-1}$ we collect about 0.3 Hz per $|t|$ -bin of $10^{-4} (\text{GeV}/c)^2$ size near $|t_{min}| = 4 \times 10^{-4} (\text{GeV}/c)^2$, using 10% acceptance. In the interference region where $|t| \simeq 1.1 \times 10^{-3} (\text{GeV}/c)^2$, the rate is down to 1.3 Hz at 60% acceptance. For the measurement of ρ and σ_{tot} not to be dominated by statistics, we need the order 10^4 events per $|t|$ -bin of $10^{-4} (\text{GeV}/c)^2$, leading to a run duration of about 30 hours.

This is also seen when one uses the interference term in the cross section: $\Delta N_i = \sqrt{N_i} \simeq 2N_0\rho\Delta\rho$, where N_i represents the number of elastic events in the interference region and N_0 the number of events when $\rho = 0$; $N_i = N_0(1 + \rho^2)$, so that, for example $\rho = 0.150$ and $\Delta\rho = 0.010$, about $(2\rho\Delta\rho)^{-2} = 1 \times 10^5$ events are needed in the interference region, which covers about five $|t|$ -bins. This simple result is corroborated by our simulation results, which indicate that $\Delta\rho \simeq 0.010$ for about 1 million events collected in $4 \times 10^{-4} \leq |t| \leq 0.2 (\text{GeV}/c)^2$.

Because of large rates, the measurement of the Coulomb amplitude will not be statistically limited, but dominated by the systematics, primarily the background estimation, acceptance calculations and uncertainty in beam angles.

Acceptance uncertainty due to the uniformity of detector response is not a problem because of the the Si detector technology implemented and already demonstrated. The main contribution is a $10\mu\text{rad}$ uncertainty in the initial beam angle, limited by the error in the BPMs at the IP, see Sec. 2.2.3.

From the experience gained from our current runs we found, that the background subtraction can be done by extrapolating non-back-to-back events to under the elastic back-to-back peak. The majority of background events is due to halo-halo coincidences and increases exponentially as the distance to the beams gets smaller.

Given the data sample of six million elastic events the statistical accuracy of the measurement of σ_{tot} is better than 1%. Therefore, the ultimate error will be limited by the systematic uncertainty on the luminosity and beam transport.

Chapter 4

Cost and Proposed Run Plan

A significant capital investment has already been made for this experiment. Four Roman Pot stations are installed and the equipment is fully debugged, including trigger and DAQ. All the accelerator controls and interfaces are in place. The collaboration is well organized.

The experiment has also obtained a three year NSF grant \$165k for support of graduate and undergraduate students and a \$40k grant to support foreign visitors from Poland. We also obtained \$98k of matching funds from the State University of New York at Stony Brook.

Given the investment already made, additional running of the experiment is very cost effective and it certainly enlarges physics output of RHIC Spin. All the costs are listed in Table 4.1. Our previous runs have shown that the experiment does not have a large impact on the accelerator itself and only short running periods are needed to accomplish our goals.

We are seeking approval of our full physics program with the understanding, that the phase two and three can be realized as additional funding becomes available. The approval of the full program will certainly allow us to seek funding for the experiment outside of the DOE, namely the NSF and participating institutions.

The experiment outlined in this proposal has three phases. The proposed timing can be arranged so that it fits the commissioning and running of RHIC with minimum impact. The cost of each phase is shown in Table 4.1.

1. In the first phase, we propose to continue measuring the elastic scattering at the current location. We propose to run at $\sqrt{s} = 200$ GeV first and 500 GeV when it becomes available.
2. In the second phase we propose to move the detectors to the location between DX and D0 magnets. A modification of the vacuum chamber in that region is required and the construction of new Roman Pot stations.
3. In the third phase, we request the run with the special high β^* optics to take data in the CNI region. The only additional cost for that phase is purchase and installation of the power supplies needed to generate the $\beta^* = 100$ m optics. It should be noted that the leads to the quadrupoles are capable to bring the higher current needed for this application as they were modified during the construction of RHIC already.

Item	\$k
Phase I	
Misc. Expense	25
Phase II	
Roman Pot Stations	160
Dx-D0 modification	100
Contingency (20%)	52
Overhead (45%)	140
TOTAL	452
Phase III	
Large β^* mods	
2000 A PS	108
2000 A PS Quench Protection	80
600 A PS	100
600 A PS Quench Protection	34
Overhead (45%)	94
TOTAL	362

Table 4.1: The cost to completion for pp2pp experiment.

Appendix A

pp2pp Paper

First Measurement of Proton-Proton Elastic Scattering at RHIC

S. Bültmann, I. H. Chiang, R. E. Chrien, A. Drees, R. L. Gill, W. Guryan,
D. Lynn, C. Pearson, P. Pile, A. Rusek, M. Sakitt, and S. Tepikian
Brookhaven National Laboratory, Upton, NY 11973, USA

J. Chwastowski and B. Pawlik
Institute of Nuclear Physics, Cracow, Poland

M. Haguenaer
Ecole Polytechnique, 91128 Palaiseau Cedex, France

A. A. Bogdanov, S. B. Nurushev, M. F. Runtzo, and M. N. Strikhanov
Moscow Engineering Physics Institute, Moscow, Russia

I. G. Alekseev, V. P. Kanavets, L. I. Koroleva, B. V. Morozov, and D. N. Svirida
Institute for Theoretical and Experimental Physics, Moscow, Russia

M. Rijssenbeck, C. Tang, and S. Yeung
Stony Brook University, Stony Brook, NY 11794, USA

K. De, N. Guler, J. Li, and N. Öztürk
University of Texas at Arlington, Arlington, TX 76019, USA

A. Sandacz
Institute for Nuclear Studies, Warsaw, Poland

(Dated: July 30, 2003)

The first result of the pp2pp experiment at RHIC on elastic scattering of polarized protons at $\sqrt{s} = 200$ GeV is reported here. The exponential slope parameter b of the diffractive peak of the elastic cross section in the t range $0.010 \leq |t| \leq 0.019$ (GeV/c)² was measured to be $b = 16.3 \pm 1.6$ (stat.) ± 0.9 (syst.) (GeV/c)⁻².

PACS numbers: 13.75Cs, 29.27Hj, 14.20Dh

Although elastic scattering has been measured in $p\bar{p}$ collisions up to $\sqrt{s} = 1.8$ TeV, the highest energy pp data reach only to 63 GeV. We present here the first measurement of the slope parameter b in forward proton-proton elastic scattering obtained by the pp2pp experiment at the Relativistic Heavy Ion Collider (RHIC) at $\sqrt{s} = 200$ GeV.

The pp2pp experiment [1] is designed to measure polarized pp elastic scattering at RHIC, which will provide proton beams with polarizations of 0.7 and luminosities up to 2×10^{32} cm⁻²sec⁻¹. The main goal of the experiment is to study the spin dependence of elastic scattering in the squared four-momentum transfer range $4 \times 10^{-4} \leq |t| \leq 1.3$ (GeV/c)² and $50 \leq \sqrt{s} \leq 500$ GeV.

By measuring elastic scattering of polarized protons in the nonperturbative regime of QCD at RHIC, one has a unique opportunity to probe the spin structure of the nucleon and of the exchanged mediators of the force, the Pomeron and its odd C-parity partner, the Odderon. The pp2pp experiment, part of the RHIC spin program, studies the physics of elastic scattering and diffractive dissociation. It addresses the main unsolved problems in

particle physics— long range QCD and confinement.

The slope b for $|t| \leq 0.5$ (GeV/c)² is inherently sensitive to the exchange process, and its dependence on \sqrt{s} will allow to distinguish among various QCD based models of hadronic interactions. Some interesting features of b observed in $p\bar{p}$ are not yet confirmed in pp elastic scattering. In general, the forward peak does not show a simple exponential behavior. The t distribution becomes less steep as $|t|$ increases from 0.02 (GeV/c)² to 0.20 (GeV/c)², although at the highest Tevatron energies this was not observed. It is therefore of interest to see the b behavior in the RHIC energy range, and also to compare the b -values for pp and $p\bar{p}$ elastic scattering. It is expected that they are the same at high energies. However the \sqrt{s} domain of RHIC is where the difference between pp and $p\bar{p}$ can still be observed.

In RHIC the two protons collide at the interaction point (IP), and since the scattering angles are small, scattered protons stay within the beam pipe of the accelerator. They follow trajectories determined by the accelerator magnets until they reach the detectors, which measure the x, y coordinates in the plane perpendicular to

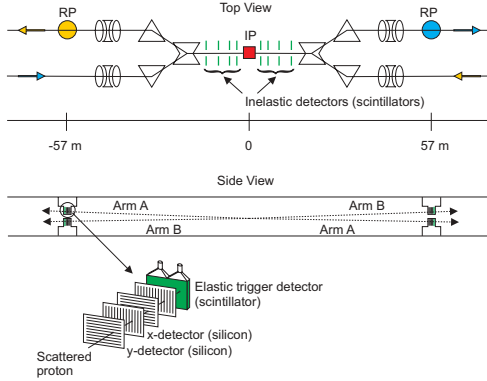


FIG. 1: Layout of the pp2pp experiment. Note the detector pairs RP and RP' lie in different RHIC rings. Scattering is detected in either one of two arms: Arm A is formed from the upper half of RP' and the lower half of RP. Conversely, Arm B is formed from the lower half of RP' and the upper half of RP.

the beam axis. The coordinates are related by the beam transport equations to the corresponding quantities at the IP:

$$\begin{aligned} x &= a_{11} \cdot x_0 + L_{eff}^x \cdot \theta_x^* + a_{13} \cdot y_0 + a_{14} \cdot \theta_y^* \\ y &= a_{31} \cdot x_0 + a_{32} \cdot \theta_x^* + a_{33} \cdot y_0 + L_{eff}^y \cdot \theta_y^* \end{aligned} \quad (1)$$

where x_0 , y_0 and θ_x^* , θ_y^* are the positions and scattering angles at the IP and a_{ij} and L_{eff} are the elements of the transport matrix. The optimum condition for the experiment is to minimize the dependence of the measured coordinates on the unknown collision vertex, i. e. to have the a_{ij} 's small and the L_{eff} 's as large as possible. In that case, called "parallel to point focusing", rays that are parallel to each other at the interaction point are focused nearly to a single point at the detector. Since in practice such a condition is achieved for one coordinate only, in our case y , Eq. (1) then simplifies to $y \approx L_{eff}^y \cdot \theta_y^*$.

The momentum-transfer interval for the data presented here is $0.004 \leq |t| \leq 0.032$ (GeV/c)². In our 14 hour run of January 2002, the RHIC orbit betatron function [2] at the IP was $\beta^* = 10$ m, resulting in $L_{eff}^y \approx 24$ m. At larger momentum transfers the acceptance is limited by the aperture of the RHIC focusing quadrupoles.

The layout of the experiment is shown in Fig. 1. The identification of elastic events is based on the collinearity criterion, hence it requires the simultaneous detection of the scattered protons in the pair of Roman Pot (RP) detectors [3], RP and RP', on either side of the IP. Additionally, a set of scintillators located outside of the beam pipe near the IP provide detection of inelastic events.

The RP's are insertion devices allowing four silicon

strip detectors (SSD) to be positioned just above and below the beam orbits. The SSD's inside the pots record the x, y coordinates of the scattered protons. The silicon detectors are made of 0.40 mm thick n-type silicon with p^+ -type implanted strips of 0.07 mm width and a strip pitch of 0.10 mm. Two of the detectors have 512 strips implanted along the longer side of the rectangle, the other two 768 strips perpendicular, resulting in an active area of 75×45 mm². Each strip is capacitively coupled to an input channel of a SVXIIe [4], which has 128 channels with preamplification, a 32 event pipeline, and a Wilkinson-type ADC.

The amount of charge collected due to a 100 GeV/c proton passing through the silicon detector corresponds to an energy deposit of about 200 keV. In 80% of the events, this deposited energy is confined to a single strip, and otherwise shared between neighboring strips if the particle passed through a $30\mu\text{m}$ wide region in between the strips.

The elastic trigger scintillators were 8 mm thick, 80×50 mm² in area, and were viewed by two photomultiplier tubes. To produce a highly efficient and uniform trigger the two signals from the tubes formed a logical OR. The elastic event trigger is a coincidence between signals in the RP's scintillators, belonging either to arm A or arm B (see Fig. 1). The trigger efficiency was greater than 0.99. For each event, time and amplitude were digitized and recorded.

The coordinate in the SSD is calculated as an energy-weighted average of the positions of the hit strips. Clusters of more than three hit strips were excluded. The detection efficiency for every SSD strip was calculated using the redundancy of the silicon planes for identification of elastic events. The average silicon detector plane efficiency for arm A was 0.97.

The collinearity of elastic events implies that the two coordinates obtained from the silicon detectors on either side of the interaction point are correlated. This correlation is shown for the y coordinates from arm A in Fig. 2. The widths of the coordinate difference distributions, σ_x and σ_y , were determined. Events for which $\sqrt{\Delta x^2 + \Delta y^2} \leq 4 \sqrt{\sigma_x^2 + \sigma_y^2}$ were retained for the analysis. The widths are dominated by the beam angular emittance of about $12\pi \mu\text{m}$ and by the uncertainty of about 60 cm (rms) in the vertex position along the beam axis.

At least six of the possible eight planes were required to have hits to be accepted for elastic events. Out of 196,000 elastic triggers for arm A about 84% were reconstructed. Most reconstruction failures are accounted for by the larger area of the scintillator compared to the active area of the SSD packages. The above mentioned correlation cut of 4σ removed another 3.8%, while the requirement of six hit planes contributing to the track reconstruction cut another 0.3%. To reduce the contami-

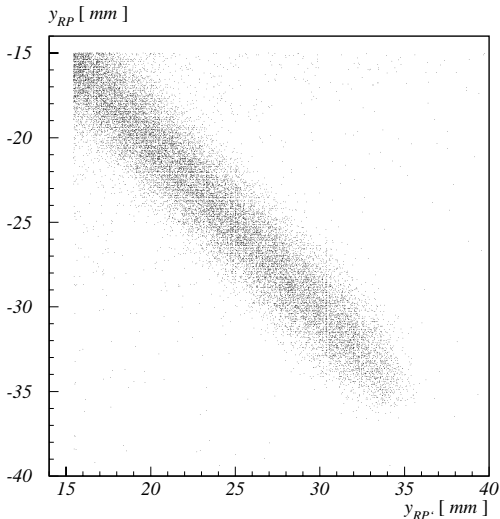


FIG. 2: Correlation between the y coordinates as measured by the two detectors of arm A for elastic events before cuts being applied.

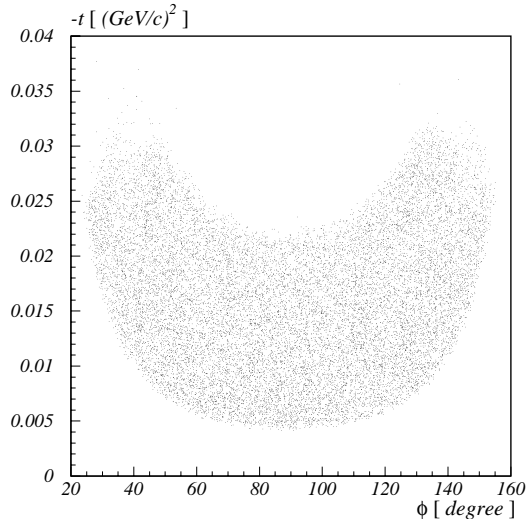


FIG. 3: Correlation between t and ϕ for reconstructed events.

nation of the elastic event sample with tracks from background particles, not more than two planes with more than one hit per event were accepted. This reduced the event sample by another 3.2%, giving a total of 153,000 elastic events for this arm. A similar analysis was carried out for arm B, but because of the noise level being considerably higher, it was used only for consistency checks, but not included in the final analysis presented here.

For each event the scattering angle θ and azimuth ϕ were calculated for each proton and then averaged. The scattering angle is related to the square of the four-momentum transfer, t , via $-t \approx (p \cdot \theta)^2$. A restriction of the ϕ range leads to a uniform geometric acceptance in a limited t -range. For $45^\circ < \phi < 135^\circ$ or $225^\circ < \phi < 315^\circ$ that range is $0.010 \leq |t| \leq 0.019 \text{ (GeV/c)}^2$. In Fig. 3 the correlation between t and ϕ is shown for reconstructed events. The determination of the slope parameter b is confined to the t region for which no acceptance correction is required. The final selection therefore yields 58,511 events. The uncorrected dN/dt distribution resulting from the ϕ -cut is shown in Fig. 4 together with the acceptance function obtained from Monte Carlo studies.

The differential cross section $d\sigma/dt$ for elastic scattering in the forward angle region is determined by Coulomb and nuclear amplitudes and the interference term between them. The cross section is given by (see for example Ref. [5])

$$\begin{aligned} \frac{d\sigma}{dt} = & 4\pi (\hbar c)^2 \left(\frac{\alpha G_E^2}{t} \right)^2 \\ & + \frac{1 + \rho^2}{16\pi (\hbar c)^2} \cdot \sigma_{tot}^2 \cdot e^{-b|t|} \\ & - (\rho + \Delta\Phi) \cdot \frac{\alpha G_E^2}{|t|} \cdot \sigma_{tot} \cdot e^{-\frac{1}{2}b|t|}, \end{aligned} \quad (2)$$

with α the fine structure constant, G_E the electric form factor of the proton, $\Delta\Phi$ the Coulomb phase[6], ρ the ratio of the real to imaginary part of the forward scattering amplitude, σ_{tot} the total cross section, and b the nuclear slope parameter. The dominant contribution in our t region is the second term in this expression.

A least squares fit was performed to the distribution of Fig. 4 using Eq. (2) with b and a normalization constant as free parameters. Since the total cross section and ρ have not been measured in this energy range, we have used values of $\sigma_{tot} = 51.6 \text{ mb}$ [7] and $\rho = 0.13$ [8]. These values of σ_{tot} and ρ come from fits to the existing pp data taken at energies below 63 GeV and world $p\bar{p}$ data. They also agree well with the predictions of other models [9], [10], [11], and [12].

The resulting slope parameter is

$$b = 16.3 \pm 1.6 \text{ (stat.)} \pm 0.9 \text{ (syst.) (GeV/c)}^{-2}.$$

The evaluation of the systematic errors due to the uncertainty in beam emittance, vertex positions and spread, beam transport matrix elements, and incoming beam an-

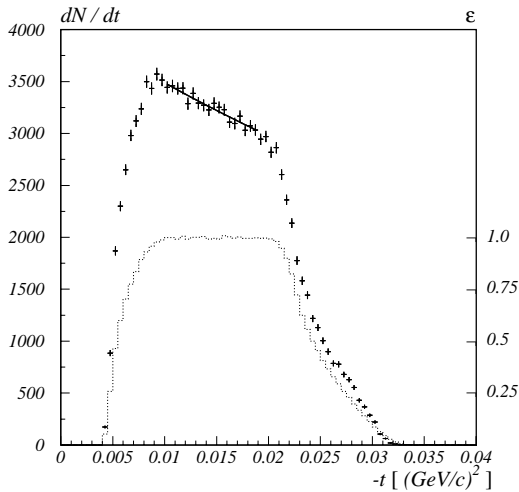


FIG. 4: The distribution of dN/dt within the ϕ region selected as described in the text. The two distributions shown are the measured data and the simulated acceptance function. The fit is shown by the solid line.

gles was based on Monte Carlo simulations. These simulations used the geometry of the experimental setup and efficiency of the detectors as an input. The largest single source of the systematic error was the uncertainty of the initial colliding beam angles.

While the horizontal component of a possible initial angle has a negligible effect on the t -distribution, the vertical component leads to an uncertainty in the absolute value of t for the reconstructed protons. This possible shift of the t -distribution scale was studied with the Monte Carlo simulation, using upper limits on the initial beam angle obtained from data. This resulted in an uncertainty on the fitted slope parameter of about 5%.

Since the fit for the slope parameter b uses nominal values for ρ and σ_{tot} our sensitivities to variations in those parameters are found to be $\delta b/\delta\rho = -16 \text{ (GeV/c)}^{-2}$ and $\delta b/\delta\sigma_{tot} = -0.018 \text{ (GeV/c)}^{-2}/\text{mb}$, respectively. Therefore changes in ρ and σ_{tot} in the order of 10 % result in changes of b which are negligible compared to statistical errors.

An independent analysis of the data was performed using different selections of hits and elastic events. In particular, a t -dependent cut on ϕ was applied, which allowed an increase in the t range and the number of accepted elastic events. The b slope values obtained from both analyses agree within statistical errors.

Our result for the slope parameter b is shown in Fig. 5 together with the world data on elastic pp and $p\bar{p}$ scattering. This result is about one standard deviation higher

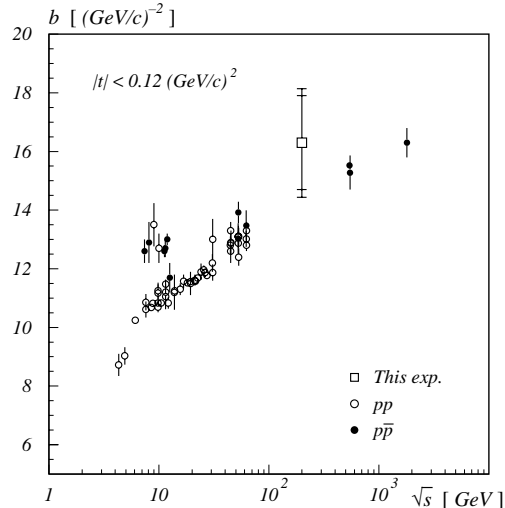


FIG. 5: The result for the slope parameter b of this experiment compared to the world pp and $p\bar{p}$ data set. The data are drawn from the Durham Database Group (UK). The error displayed for our result shows both statistical and total errors, where the latter has been computed by a quadrature sum.

than an extrapolation of world data to the energy of this experiment [7], [9], [10]. It agrees well with model predictions [12], [13].

In the future, a full complement of two sets of Roman Pot detector pairs will be used, two pairs at each side of the IP, to allow a direct measurement of the scattering angles. This will reduce the systematic error due to the uncertainty of the vertex position. An expected increase of the RHIC luminosity will result in a reduction of the statistical error and will make the studies of the polarized observables A_N and A_{NN} feasible.

The research reported here has been performed in part under the US DOE contract DE-AC02-98CH10886, and was supported by the US National Science Foundation and the Polish Academy of Sciences. The authors are grateful for the help of N. Akchurin, D. Alburger, P. Draper, Y. Onel, A. Penzo, and P. Schiavon at an early stage of the experimental design and the support of the BNL Physics Department, Instrumentation Division, and C-A Department at the RHIC-AGS facility.

-
- [1] W. Guryn *et al.*, RHIC Proposal R7 (1994) (unpublished); V. Kanavets, Czech. J. Phys., Suppl. A, **53**, A21 (2003)
 [2] M. A. Harrison, The RHIC Project, Fifth European Par-

- ticle Accelerator Conference, Geneva (1996)
- [3] R. Battiston *et al.*, Nucl. Instr. Meth. **A238**, 35 (1985)
 - [4] R. Lipton, Nucl. Instr. Meth. **A418**, 85 (1998)
 - [5] U. Amaldi *et al.*, Phys. Lett. **B43**, 231 (1973)
 - [6] B. Z. Kopeliovich and A. V. Tarasov, Phys. Lett. **B 497**, 44 (2001).
 - [7] A. Donnachie and P. V. Landshoff, Phys. Lett. **B296**, 227 (1992)
 - [8] C. Augier *et al.* (UA4/2 collab.), Phys. Lett. **B316**, 503 (1993)
 - [9] Martin M. Block, Nuc. Phys **B** (Proc. Suppl.) **71**, 378 (1999)
 - [10] B. Z. Kopeliovich, I. K. Potashnikova, B. Povh, and E. Predazzi, Phys. Rev. **D63** 054001 (2001)
 - [11] V. V. Ezhela *et al.* (COMPETE collab), Phys. Rev. **D65** 074024, (2002)
 - [12] C. Bourrely and J. Soffer, Euro. Jour. Phys. **C28**, 97, (2003)
 - [13] J. Soffer, private communication (2003)

Appendix B

Bibliography

Bibliography

- [1] W. Guryn *et al.* (pp2pp Collaboration), *Experiment to Measure Total and Elastic pp Cross Sections at RHIC*, RHIC Proposal R7 (1994), unpublished.
- [2] L. N. Lipatov, Sov. Phys. JETP **63** (1986) 904.
- [3] F. E. Low, Phys. Rev. **D12** (1975) 163.
- [4] S. Nussinov, Phys. Rev. Lett. **34** (1975) 1286.
- [5] V. S. Fadin, E. A. Kuraev, and L. N. Lipatov, Phys. Lett. **B80** (1975) 50.
- [6] L. Łukaszuk and B. Nicolescu, Il Nuovo Cim. Lett. **8** (1973) 405.
- [7] P. Gauron, E. Leader, and B. Nicolescu, Phys. Rev. Lett. **54** (1985) 2656.
- [8] D. Joynson, E. Leader, and B. Nicolescu, Il Nuovo Cimento **30** (1975) 345.
- [9] P. Gauron, E. Leader, and B. Nicolescu, Phys. Lett. **B397** (1997) 126.
- [10] M. G. Ryskin, Yad. Fiz. **46** (1987) 611 [Sov. J. Nucl. Phys. **46** (1987) 337].
- [11] A. Donnachie and P. V. Landshoff, Nucl. Phys. **B348** (1991) 297.
- [12] C. Ewertz, *The Odderon in Quantum Chromodynamics*, hep-ph 0306137 (2003).
- [13] M. Jacob and G. C. Wick, Ann. Phys. (N.Y.) **7** (1959) 404.
- [14] J. Schwinger, Phys. Rev. **73**, 407 (1948); B. Z. Kopeliovich and L. I. Lapidus, Yad. Fiz. **19** (1974) 218 [Sov. J. Nucl. Phys. **19** (1974) 114].
- [15] N. H. Buttimore, E. Gotsman, and E. Leader, Phys. Rev. **D18** (1978) 694.
- [16] B. Z. Kopeliovich and B. Z. Zakharov, Phys. Lett. **B226** (1989) 156.
- [17] C. Bourrely and J. Soffer, *How to calibrate the polarization of a high energy proton beam? A theoretical prospect*, Spin 96, *op. cit.* pp. 825.
- [18] N. H. Buttimore *et al.*, Phys. Rev. **D59** (1999) 114010.
- [19] G. Fidecaro *et al.*, Phys. Lett. **B76** (1978) 369.

- [20] J. H. Snyder *et al.*, Phys. Rev. Lett. **41** (1978) 781.
- [21] M. Corcoran *et al.*, Phys. Rev. **D22** (1980) 2624.
- [22] R. V. Kline *et al.*, Phys. Rev. **D22** (1980) 553.
- [23] G. Fidecaro *et al.*, Phys. Lett. **B105** (1981) 309.
- [24] M. Borghini *et al.*, Phys. Lett. **31B** (1970) 405.
- [25] M. Borghini *et al.*, Phys. Lett. **36B** (1971) 501.
- [26] G. W. Abshire *et al.*, Phys. Rev. Lett. **32** (1974) 1261.
- [27] A. Gaidot *et al.*, Phys. Lett. **B61** (1976) 103.
- [28] D. G. Crabb *et al.*, Phys. Rev. Lett. **41** (1978) 1257.
- [29] D. G. Crabb *et al.*, Phys. Rev. Lett. **65** (1990) 3241.
- [30] K. Hinotani *et al.*, Nuovo Cimento **A52** (1979) 363.
- [31] N. Akchurin, N. Buttimore, and A. Penzo, *Spin-Flip in Elastic and Diffractive Scattering*, Vth Blois Workshop, Providence, Rhode Island, June 1993.
- [32] M. Anselmino and S. Forte, Phys. Rev. Lett. **71** (1993) 223.
- [33] E. Leader, *Proc. of LHC Workshop (Aachen)*, CERN 90-10 Vol.2 (1990) 22.
- [34] N. Akchurin *et al.*, Phys. Lett. **B29** (1989) 299.
- [35] N. Akchurin *et al.*, Phys. Rev. **D48** (1993) 3026.
- [36] E. Leader and T. L. Trueman, Phys. Rev. **D61** (2000) 077504.
- [37] A. Donnachie and P.V. Landshoff, Phys. Lett. **B1296** (1992) 227.
- [38] M. M. Block, Nucl. Phys. **B71** (Proc. Suppl.) (1999) 378.
- [39] A. Martin, *Proc. of International Conference on Elastic and Diffractive Scattering*, eds. M. M. Block and A. R. White (1989), 1–8.
 F. Halzen, Summary Talk Blois V, *Proc. of International Conference on Elastic and Diffractive Scattering, June 1993, Brown U., Providence, USA*, eds. H. M. Fried, K. Kang, C-I. Tan, World Scientific 1994. M. Albrow, Experimental Summary Blois V, *Proc. of International Conference on Elastic and Diffractive Scattering, June 1993, Brown U., Providence, USA*, eds. H. M. Fried, K. Kang, C-I. Tan, World Scientific 1994.
- [40] W. Kienzle *et al.* (TOTEM Collaboration), Letter of Intent *Total Cross Section, Elastic Scattering and Diffraction Dissociation at the LHC* (1997), unpublished.

- [41] E. Nagy *et al.*, Nucl. Phys. **B150** (1979) 221.
- [42] C. Bourrely, J. Soffer and T. T. Wu, Z. Phys. **C37** (1988) 369;
C. Bourrely and J. Soffer, Euro. Jour. Phys. **C28** (2003) 97.
- [43] R. J. Glauber and J. Velasco, Phys. Lett. **B147** (1984) 380.
- [44] R. J. M. Covolan *et al.*, Z. Phys. **C58** (1993) 109.
- [45] A. Donnachie and P. V. Landshoff, Nucl. Phys. **B267** (1986) 690.
- [46] P. Desgrolard, M. Giffon and E. Predazzi, LYCEN 9339 (1993), unpublished.
- [47] A. Breakstone *et al.*, Phys. Rev. Lett. **54** (1985) 2180.
- [48] P. V. Landshoff, Proc. of the 1991 HEP Conference, Geneva, 1991.
- [49] M. Bozzo *et al.*, Phys. Lett. **B155** (1985) 197.
- [50] D. Bernard *et al.*, Phys. Lett. **B171** (1986) 142.
- [51] N. A. Amos *et al.*, Phys. Lett. **B247** (1990) 127.
- [52] E.D. Courant and H.S. Snyder, Annals of Physics: **3** (1958) 1.
- [53] R. Gupta, BNL, private communications.
- [54] R. Lipton, Nucl. Instr. Meth. **A238** (1985) 35.
- [55] B. Z. Kopeliovich *et al.*, Phys. Rev. **D63** (2001) 054001.
- [56] R. Battiston *et al.*, Nucl. Instr. and Meth. **A238** (1985) 35.